Local structural investigation of Ca & Sr doped $LaAlO_3$ perovskite

Thesis submitted for fulfillment of the requirements for the degree of

Master of Technology in

Nano Science & Technology

Jadavpur University

Submitted by

Rabiul Naiya

Exam roll no: M4NST24019

Registration no: 156290 of 2020-21

Under the joint guidance of

Dr. Jiten Ghosh	**Dr. Chandan Kumar Ghosh**
Sr. Principal Scientist	*Assistant Professor*
Material Characterization Division	School of Materials Science and Nanotechnology
CSIR- Central Glass and Ceramic Research Institute,	Jadavpur University
Kolkata-700032	Kolkata - 700032

November, 2024

CERTIFICATE OF RECOMMENDATION

This is to certify that the thesis entitled "Local structural investigation of Ca & Sr doped $LaAlO_3$ perovskite" is done by **RABIUL NAIYA** under the supervision and guidance for partial fulfillment of the requirement of master of Technology in nano Science and Technology in School of Materials Science and nanotechnology, Jadavpur University during the academic session 2022-2024.

Dr. Jiten Ghosh

Sr. Principal Scientist

Material Characterization Division

CSIR-Central Glass and Ceramics Research Institute, Kolkata

(Guide)

Dr. Chandan Kumar Ghosh

Assistant Professor

School of Material Science and Nanotechnology

Jadavpur University

(Co-Guide)

DEAN

Faculty Council of interdisciplinary

Studies Law and Management

Kolkata -700032

HOD/Director

Dr. Mahua Ghosh,

School of Material Science and Nanotechnology

Jadavpur University

Kolkata -700032

Certificate of approval

The thesis is hare by approved as a credible study of an engineering subject carried out and represented in a satisfactory manner to warrant its acceptance as a prerequisite to the degree for which it has been submitted.

It is to be understood that by this approval the undersigned does not necessarily endorse or approved any statement made opinion expressed or conclusion drawn there in but approved the thesis only for the purpose for which it has been submitted.

Signature of the Examiner

……

……

……

……

DECLARATION OF ORIGINALITY AND COMPLIANCE OF ACADEMIC ETHICS

I hereby declare that, this literature contains survey and original research work by the undersigned candidate as part of Master of Technology (Nano-science and Technology) studies during academic session 2022-2024.

All the given information in this document has been obtained and presented in accordance with academic rules and ethical conduct.

I also declare that, as require by this rules and conduct, I've completely cited and referred all information and results are original to this work.

Name : Rabiul Naiya

Roll no : M4NST24019

Thesis Title : Local structural investigation of Ca & Sr doped $LaAlO_3$ perovskite

ACKNOWLEDGEMENT

While bringing out this thesis paper to its final form, I came across a many people whose contributions in various ways helped me to understand my field of knowledge and research and they deserve special thanks for that. It is a pleasure to convey my gratefulness to all of them.

I would like to express my sincere and heartfelt gratefulness to my guides Dr. Jiten Ghosh (CSIR-CGCRI) & Co-guide Dr. Chandan Kumar Ghosh (Jadavpur University) for sharing their knowledge with me, guiding me in my work at CSIR CGCRI & Jadavpur University. The ideas and guidance they have provided me are invaluable. Their motivation has helped me to finish my thesis work in proper way.

I also express sincere gratitude to the Director, CSIR-CGCRI, Kolkata for provide me with an opportunity to undergo my M. Tech project at CSIR- CGCRI, Kolkata. I am also thankful to Dr.Tarun Kumar Kayal (chief scientist & head MCD), for giving this opportunity to work in the Material Characterization Division of CSIR-CGCRI.

I would like to thank Dr. Jiten Ghosh for his assistance to carry out different experiments at MCD division. I would like to thank Dr. Santanu Sen, Mr. Prosenjit Khan, Mr. Sumit Nath, Kanchan Kole, Akash Ali Mallick, Subash Sharma and Asish Jana for their never-ending support and for keeping such memorable assessment. I would like to thanks all the staff members of Material Characterization Group. I would like to thanks each and everyone else who helped me in the completion of my project.

I am also grateful to all my classmates, who always gave me a constant co-operation and support throughout the project work. I am also thankful to all the stuff members of the department for their full co-operation and much needed help.

My greatest thanks are to all who wished us success especially my parents and friends whose support and care make our stay on Earth.

Contents

Chapter:1 Introduction

1.1 **Introduction on Nano-science and Nanotechnology:** 4-5

1.2 **General Overview on Lanthanum aluminate (LaAlO3) perovskite** 5-6

Chapter 2 :Literature review 7-10

Chapter 3: Materials and Methods

3.1 Sample preparation 11

3.1.1 Planetary ball milling 12

3.1.2 Furnace 12

3.2 Characterization techniques

3.2.1 X-Ray diffractometer (XRD) 13

3.2.2 FESEM (Field-emission Scanning Electron Microscope) 14

3.2.3 Di-electric Measurement 15

3.2.4 TGA and DTA 15

Chapter 4 : Synthesis and characterization of LaAlO3 nano powders

4.1 Sample preparation 16

4.2 Product characterizations

4.2.1 X-ray diffractometer (XRD) 16-19

4.2.2 FESEM Analysis 16-20

4.2.3 Dielectric measurement 21

4.2.4 TG/DTA analysis 22

Chapter 5 : Synthesis and characterization of Ca doped LaAlO3 ($La_{0.8}Ca_{0.2}AlO_3$)nano powders .

5.1 Sample preparation 23

5.2 Sample characterizations

5.2.1 X-ray diffractometer (XRD) 23-26

5.2.2 FESEM Analysis 26

5.2.3 Dielectric measurement 27

5.2.4 TG/DTA analysis 28

Chapter 6 : Synthesis and characterization of Sr doped LaAlO3 ($La_{0.8}Sr_{0.2}AlO_3$)nano powders

6.1 Sample preparation 30

6.2 Sample characterizations

6.2.1 X-ray diffractometer (XRD) 30-33

6.2.2 FESEM Analysis 34

6.2.3 Dielectric measurement 35

6.2.4 TG/DTA analysis 36

Chapter 7: Conclusion..... 37

Abstract

In this work, Lanthanum aluminate ($LaAlO_3$), $La_{0.8}Ca_{0.2}AlO_3$ (LCAO) and $La_{0.8}Sr_{0.2}AlO_3$ (LSAO) have been prepared by high energy ball milling with different ball milling hours (25hours,50hours,75 hours and 100 hours) to study the local distortion in lattice due to presence of dopants (Ca and Sr).We used simple materials lanthanum oxide (La2O3)(99.98%) Sigma-Aldrich),aluminum oxide(Al2O3)(99% Sigma-Aldrich),calcium oxide(CaO) and strontium carbonate(SrCO3) to create this powders, we heated it at 900°C to complete the process. It was characterized by several techniques: X-ray diffraction (XRD), Field-emission Scanning Electron Microscope (FESEM), LCR meter, thermogravimetric and differential thermal analysis (TG/DTA). X-ray diffraction (XRD) confirmed that $LaAlO_3$ samples changing their phase from hexagonal to cubic structure slowly with increasing ball milling hours and Ca doped LaAlO3 shows existence of secondary phase(unwanted impurity CaCO3) which play vital role in dielectric measurement. Field-emission Scanning electron microscopy (FESEM) reveals very fine clusters of nanosized spherical particles and the product is highly agglomerated with increasing ball milling hours. Dielectric constant of $LaAlO_3$ is found to be 30-12. The dielectric property depends on this local atomic arrangement of Ca and Sr atoms in $LaAlO_3$ and coexistence of multiple phases. A tiny amount of dopant (like Sr or Ca) can significantly change how materials work, including their electrical conductivity and dielectric constant. We will study how the $LaAlO_3$ powder changes as the particle size gets smaller and then connect the dielectric properties to the structure at the nano-scale since electronic devices are becoming more miniaturized.

Keyword: $LaAlO_3$, Ca doped $LaAlO_3$,Sr doped $LaAlO_3$, XRD, Local Structure, High energy ball milling, FESEM, Dielectric measurement, TG/DTA.

Chapter:1 Introduction

1.1 Introduction to Nano-science and Nanotechnology:

Nanotechnology indeed represents a transformative field that operates at the nanometer scale, allowing precise manipulation of materials at atomic and molecular levels. This technology opens pathways to develop new materials and devices with unique properties, offering potential solutions across diverse fields, including medicine, electronics, energy, and environmental science.Nanotechnology also plays a critical role in energy and environmental sectors. Nanotechnology is rooted in the ability to manipulate materials at the atomic and molecular scale, typically in the range of 1 to 100 nanometers. At this scale, materials exhibit unique properties due to quantum effects and increased surface area, which differ drastically from those of bulk materials. These properties include changes in optical, mechanical, magnetic, thermal, and electrical behaviors, making nanomaterials highly desirable for a wide range of applications. Nanostructured materials can improve the efficiency of solar cells, enable better catalysts for cleaner chemical processes, and contribute to advanced filtration systems for water purification [1].

Fundamental Concepts and Origins of Nanotechnology

The concept of nanotechnology was indeed introduced by the American physicist Richard Feynman, who is often considered the father of modern nanotechnology. In his pioneering 1959 lecture at Caltech, titled "There's Plenty of Room at the Bottom, “Feynman envisioned the potential for manipulating matter at the atomic and molecular scale. He famously asked, “Why can’t we write the entire 24 volumes of the Encyclopedia Britannica on the head of a pin?"—highlighting the possibility of storing vast amounts of information in a tiny space. In his visionary talk, he described building increasingly smaller machines down to the molecular level, an idea that has become central to nanotechnology today. It wasn’t until 1974 that Japanese scientist Norio Taniguchi formally coined the term "nanotechnology." Taniguchi defined it as "mainly consisting of the processing of separation, consolidation, and deformation of materials by one atom or one molecule." His definition laid the groundwork for nanotechnology as a distinct scientific field focused on manipulating materials at the atomic and molecular levels. Together, Feynman and Taniguchi set the conceptual and linguistic foundations of a field that has since evolved into a multidisciplinary domain with transformative applications across multiple scientific and technological areas. [2].

Properties of Nanomaterials

1. Shape and Size: The physical dimensions of nanomaterials, including their shape and size, directly influence their properties and applications. For instance, nanoparticles can be spherical, tubular, or irregularly shaped, and these forms determine their interactions with other materials and systems.

2. Surface Charge and Stability: The surface charge of nanomaterials affects their colloidal stability, reactivity, and interactions with biological systems. Proper surface functionalization can enhance stability and reduce aggregation, making nanomaterials more effective in various applications.

3. Quantum Size Effect: At the nanoscale, quantum confinement can alter the electronic properties of materials, leading to unique optical and electronic behaviors that are not observed in bulk materials.

4. Optical Properties: Nanomaterials can exhibit unusual optical properties, such as enhanced fluorescence or plasmon resonance, which are useful in applications like bioimaging and sensing.

5. Thermal and Electrical Properties: Nanomaterials can have enhanced thermal conductivity and electrical properties, making them valuable in electronics and energy applications [3].

Classification of Nanomaterials

Nanomaterials are systematically classified based on their configuration and dimensionality:

0D (Zero-Dimensional): Nanoparticles with no extended dimensions (e.g., quantum dots).

1D (One-Dimensional): Nanomaterials extended in one dimension (e.g., nanowires, nanotubes).

2D (Two-Dimensional): Materials extended in two dimensions (e.g., graphene, nanosheets).

3D (Three-Dimensional): Materials in all three dimensions (e.g., nanostructured foams)[4].

1.2 General Overview on Lanthanum aluminate (LaAlO3)

LaAlO3 has a perovskite-type structure, which is known for its versatility in accommodating various ions, leading to a wide range of physical properties. This structure is crucial for its use in different applications.Its perovskite-like crystalline structure lends itself to a variety of technological applications, particularly in areas that require specific electrical and magnetic properties shown in Table 1.

Table 1: Properties of $LaAlO_3$

Property	**Value**	**Referenance**
Optical Band gap	6.1 eV	[5]
Thermal expansion coefficient	9.4x10-6 / deg C	[6]
Dielectric Constant	27	[7]
Loss tangent (10 GHz)	3 x 10-4 @ 300K, 0.6 x 10-4 @ 77K	[8]

Application:

1. **Substrate for Superconductors**: LaAlO3 is commonly used as a substrate for high-temperature superconducting films. Its excellent lattice and thermal expansion matching with other materials, like YBa2Cu3O7 (YBCO), make it ideal for this purpose. This matching is critical in maintaining the integrity and performance of superconducting films [9].

2. **Electrical Insulation**: LaAlO3 is used as an electrically insulating buffer layer. Its high dielectric constant and good insulating properties make it suitable for separating conductive layers in electronic devices.

3. **Gate Dielectric Material**: There has been research into using LaAlO3 as a gate dielectric material in transistors. Its high dielectric constant could potentially lead to the development of smaller, faster, and more energy-efficient electronic devices.

4. **Ferroelectric and Magnetic Properties**: LaAlO3 can exhibit interesting ferroelectric and magnetic properties when doped or combined with other materials. These properties are valuable in the development of various electronic and spintronic devices [10].

Chapter 2 : Literature review

[1] Guoheng Qin.et.al. were successfully synthesized $LaAlO_3$ nanopowders and double-doped by Sr and Mg with homogenous composition. Single phase $LaAlO_3$ solid solution is synthesized at 750 °C for 3h, which is converted from amorphous precursor powders without any intermediate phase formation. After calcined at 1000 °C for 3 h, the particle size of La0.90Sr0.1Al0.97Mg0.03O3 (LSAM) is 136 nm measured by APS. The maximum shrinkage value of 20.6 percent and relative density of 95 percent are obtained sintered at 1600 °C for 5 h for 1000 °C-calcined LSAM powders. The total conductivity of 7.87 × 10 3 S cm 1 at 800 °C for LSAM electrolyte is measured by AC impedance spectroscopy and powders possess excellent sinterability[11].

[2] Taku Onishi was successfully synthesized Sr doped $LaAlO_3$ nanopowders .When Sr-doped with LaAlO3 perovskite ,the activation energy decrease in strontium-doped LaAlO3 by the cluster model calculations based on hybrid density functional theory. The binding energy in Sr-O_{cond} bond are smaller than that in La-O_{cond} that's why the activation energy for oxide ion conduction becomes smaller.Also Sr-doped LaAlO3 Affects the covalent and ionic bonds between counter cation and conductive oxide ion which is respon-sible for the activation energy change[12].

[3] Neelapala.et.al, were synthesized La1-xSrxAlO3 (x=0 to 0.4) perovskite by reverse strike co-precipitation method . XRD shows that La1-xSrxAlO3 perovskite from x=0 to 0.35 exist rhombohedral phase, while for La0.6Sr0.4AlO3 sample the secondary phases SrO, La2O3, and Al2O3 were also noticed. Sr-doped samples exhibited higher BET specific surface area than LaAlO3. FESEM showed that there is a change in morphology upon doping of Sr into LaAlO3 lattice. XPS confirmed the existence of La, Sr and Al in +3, +2 and +3 oxidation states, La0.75Sr0.25AlO3 exhibited higher amount of adsorbed oxygen species due to the gen- eration of more oxygen vacancies[13].

[4] Martin Fabián.et.al. were synthesized Ca-substituted La1-xCaxAlO3- (x=0.05–0.20) perovskites by mechanosynthesis route. XRPD showed formation of perovskite phase after 30 min of ball milling. Sintering at 1450°C yielded dense ceramics with relative density above 95 %. Refinement of XRPD data revealed a decrease of lattice constant with increasing calcium content. XPS confirmed Ca replacing La cations in their twelve-coordinated positions. EDX confirmed average cation composition very close to the nominal. Substitution of Ca increases total electrical conductivity by 2–3 orders of magnitude compared to undoped LaAlO3 in air. In this series, partial oxygen-ionic conductivity increases Oxygen- ionic contribution to the total conductivity is 20–68% at 900°C. Impedance spectroscopy shows electrical properties of La1-xCaxAlO3- ceramics below 800°C are determined by grain boundary[14].

[5] Joel Zylberberg.et.al. were synthesized Bismuth-doped LaAlO3 was prepared in the form of solid solu-tion, La1xBixAlO3 0x0.2, by solid-state reactions. The materials were characterized by x-ray diffraction and dielectric spectroscopy. With increasing bismuth amount x, the dielectric con- stant increases from 31.6 for pure LaAlO3 to 34.6 for x=0.2, while the loss tangent drops from 0.03 to 0.004 f =100 Hz. The frequency dispersion of the dielectric constant is attenuated. The improved dielectric properties in the Bi-doped LaAlO3 are attributed to the high polarizability of Bi3+ ion with a lone electron pair[15].

[6] Jie Yang.et.al. The nonmetallic Si4+ doped modified lanthanum aluminate (LaAlO3) solid electrolyte for the first time, which has particular scientific significance, and La1 -xSrxAlO3 material was successfully prepared by the sol–gel method.La1-xSrxAlO3 is a ceramic material sintered at 1100C for 2 h in an air atmosphere. The surface microstructure and electrochemical properties of the samples were tested by multiple characterization methods. The results show that the La1-xSrxAlO3 has good sintering activity, high crystallinity, and a grain radius of approximately

25 nm. At 800C, the ionic conductivity is above 1.05E 04 Scm and the activationenergy is lower than 1.19 eV[16].

[7] Te-Yuan Chen.et.al.were doped LaAlO3 with various types of divalent cations are Ba,Ca and Sr.The objective was to investigate the effect of dopants on the crystal structure and con- ductivity of LaAlO3. As a result, the solubility of Ca ion into the La cation sublattice wasfound to be 5 mol percent and the solubility of Sr ion could reach 20 mol percent. However, only less than 1 mol percent Ba ion could be dissolved. In this study, Mg ion was substituted for Al ion in the B-site. The solubility of Mg ion was about 3 mol percent. With double doping for A and B parent cations, the addition of Ca, Sr, Ba ion tend to enhance the solubility ofMg ion from 3 to 10 mol percent. Although the addition of Mg ion increased the solubility of Ca ion, the solubility of Sr and Ba ion was suppressed. The concentration of oxygen vacancy increases with the increasing amount of divalent cation dopants, within their solubility lim-its. However, the second phases were found to be stoichiometric compounds without oxygen defects. Thus, the conductivity of second phases was significantly lowered. In the LaAlO3 per- ovskite systems, the activation energies for ionic conduction were also significantly influenced by the addition of dopants. The activation energy for singly and doubly doped samples, were about 89–108 and 90–126 kJ/mol, respectively, which is lower than that for undoped LaAlO3is 127 kJ/mol[17].

[8] Lúcia Adriana.et.al. investigated the impact of Sr and Mn co-doping on LaAlO3, focusing on microstructural evolution and electrical properties. Here are the key findings from the research.The addition of Sr contributes to the crystallization and stabilization of the per- ovskite structure of LaAlO3. However, it also leads to the formation of a heterogeneous microstructure when added alone.When Sr and Mn are co-doped into LaAlO3, they synergis- tically improve the homogeneity of Al and La within the perovskite structure. This indicatesa more uniform distribution of these elements throughout the material.The addition of Sr alone significantly enhances the electrical conductivity of LaAlO3. Specifically, the electri- cal conductivity at 600 °C for La0.8Sr0.2AlO3- is reported to be 5.74 × 104 S/cm, which is three orders of magnitude higher than undoped LaAlO3 (2.96 × 106 S/cm at 600 °C).Mn co-doping further enhances the electrical conductivity beyond what Sr doping achieves alone. For La0.8Sr0.2Al0.8Mn0.2O3-, the electrical conductivity at 600 °C is 3.6 × 102 S/cm, whichis five orders of magnitude higher than undoped LaAlO3[18].

[9] Villas-Boas.et.al. werw studied on pure LaAlO3 and its variants doped with Sr, Ba, and Ca. These powders were synthesized using the solid-state reaction method. The microstructural, structural, and electrical properties of the sintered samples were examined through scanning electron microscopy, X-ray diffraction, and impedance spectroscopy. Among the various dopants, the Sr-doped sample exhibited the highest conductivity at 800°C for both grain and total conductivity. In all doped samples, the grain boundary was identified as more resistive than the grain, leading to the total conductivity being controlled by the grain bound- ary. The microstructures of these materials were heterogeneous, with the level of heterogeneityinfluenced by the type of dopant used[19].

[10] Anthony H. McDaniel.et.al.were reported nonstoichiometric perovskite oxides for solar-thermochemical water and carbon dioxide splitting cycles. LaAlO3 doped with Mn and Sr efficiently splits both gases, producing hydrogen yields 9 times greater and carbon monoxide yields 6 times greater than ceria, the current top material. The perovskite also evolves oxygen at 300 °C lower than ceria and remains robust over at least 80 CO2 splitting cy- cles. These findings are crucial for developing efficient concentrated solar fuel technologies[20].

[11] Anastasia V. Egorova.et.al.were calculated the electrical properties of LaAlO3 perovskite doped with zinc, forming a new solid solution LaAl1-xZnxO3-1/2x through a solid state reaction. The study finds that the undoped LaAlO3 has a rhombohedral crystal structure, while the doped version exhibits cubic symmetry. The doping homogeneity is limited to a maximum concentration of 5 mol. percentage of Zn. Computational simulations and experimental results indicate that LaAlO3 has high energy barriers for oxygen ion transport, correlatingwith its low electrical conductivity. However, substituting Al with Zn increases conductivity by approximately two orders of magnitude with the electronic

This enhancement in electrical properties suggests potential applications in electrochemical devices such as solid oxide fuel cells [21].

[12] Ji Young Park.et.al, were studied the electrical conductivity of LSAM9191 (10 percentage of Sr and10 percentage of Mg doped LaAlO3) from 400 to 1000 °C using impedance spec- troscopy. Conductivity was also measured as a function of oxygen partial pressure (PO2) be- tween 800 and 1000 °C. Below 550 °C, grain boundary resistance dominated conductivity, which decreased significantly above 800 °C. LSAM9191 behaved as an oxygen ion conductor at low PO2 and a mixed conductor at high PO2 in the temperature range influenced by grain proper- ties. The ionic conduction region expanded slightly with temperature, indicating LSAM9191's potential as a high-temperature oxygen ion conductor in low PO2 environment[22].

[13] Cristiane A. da Silva.et.al. were synthesized and characterized of undoped, Sr-doped, Mn-doped and (MnSr)-codoped LaAlO3 powders produced using the Pechini method. The synthe- sis was designed to produce powders that meet the requirements such as particle size control, high surface area, stoichiometric control and morphology suitable for the production of ce- ramic suspensions to be processed into an SOFC anode. The powders were analyzed using several physical and chemical characterization techniques such as XRD, XRF, TGA/DTA, SEM, TEM, BET, FTIR, XPS and H2-TPR. The results have shown that all the calcined samples studied exhibited single-phase perovskite structures possessing relatively high sur- face energy with nano-sized particles. Thermal analysis and FTIR results provided the basis for choosing 900 °C as the calcination temperature. Thermal expansion coefficients for the undoped and doped lanthanum aluminate matched very well that of the conventional yttria stabilized zirconia electrolyte. Among the different compositions studied, the Mn-doped, as well as the (MnSr)-codoped electrocatalysts, exhibited a sufficiently high electrical conductiv- ity for SOFC application.[23].

[14] Aliza Zahoor.et.al. examined DFT-based structural and elastic proper-ties of pure and Be-doped LaAlO3, with Be incorporated at both La-sites and Al-sites (La1- xBexAlO3 and LaAl1-xBexO3, x = 0 percent, 20 percent, 40 percent, 60 percent, 80 percent,and 100 percent). Supercell calculations reveal that Be doping alters lattice parameters, sig- nificantly impacts band structure, and changes electronic properties. Be doping at La-sites leads to metallic conductivity, while at Al-sites, it increases the band gap from 3.01 eV to 3.31 eV and shifts it from indirect to direct. Elastic property analysis shows Be-doped structuresare mechanically stable and more ductile. The study of mean sound velocity and Debye tem- perature indicates weaker bonding and lower thermal conductivity than pure LaAlO3. These changes make the doped material suitable for various applications. Additionally, pressure- induced structural properties of pure and Be-doped LaAlO3 are considered[24].

[15] L.Djoudi.et.al. were synthesized Lanthanum monoaluminate (LaAlO3) using the co-precipitation method with NaOH, La(NO3)3·6H2O, and Al(NO3)3·9H2O as raw materials. The synthesized powder was calcined at different temperatures and characterized using severaltechniques, including Fourier Transform Infrared Spectroscopy (FT-IR), Thermogravimetric and Differential Thermal Analysis (TGA/DTA), X-ray Diffraction (XRD), and laser diffusion. The results indicated that the crystallization temperature of the LaAlO3 precursor gels, as determined by TG/DTA, was approximately 790°C. The XRD pattern of the LaAlO3 precursor gels calcined at 700°C for 6 hours revealed a perovskite structure with a rhombohedral hexagonal phase and no crystalline impurities. Additionally, the crystallite size of LaAlO3increased from 31 nm to 44.5 nm as the calcination temperature was raised from 700°C to 1000°C for 6 hours[25]

[16] Abdelkader Boudali.et.al. were investigated at T=0 K the structural,elastic,and electronic properties of the perovskite insulator LaAlO3 have been conducted using both full- potential linearized augmented plane wave (FP-LAPW) and pseudopotential plane-wave (PPs- PW) methods. The exchange-correlation potential was evaluated using the generalized gradient approximation (GGA) and local density approximation Tr-Blaha + mBJ. Ground-state pa- rameters such as lattice parameter, bulk modulus, its pressure derivative, and elastic constants were determined and found to align well with theoretical predictions and available experimental data. Analysis of the partial contribution of each atom to the total density of states was performed, LaAlO3 to be an insulator with a direct band gap close to 98 percent of the experi- mental value. This electronic characteristic necessitates a re-evaluation of its optical propertiesalso thermodynamic properties were explored using the Debye quasiharmonic model, indicat- ing that the predicted heat capacity Cv approaches the Dulong-Petit limit[26].

[17] Pawan Kumar.et.al. were synthesized a single-phase perovskite LaAlO3:Dy3+ phosphor via a gel-combustion method at 600°C using hexamethylenetetramine as a fuel.Subsequent cal- cination steps at 800°C and 1000°C were employed to explore their impact on crystalline structure and luminescent properties. The Xrd data shows us the structure is a cubic unit cell.Debye–Scherrer and Williamson–Hall equations were utilized to analyze particle size and structural features. TEM revealed the morphology and particle dimensions. FTIR identified metal–oxygen vibration modes, complementing diffraction findings. Energy-dispersive X-ray analysis verified the chemical composition. Luminescence spectra of LaAlO3:Dy3+ phosphors demonstrated intense emissions at 482nm (bluish) and 574nm (yellowish) corresponding to 4F9/2→6H15/2 and 4F9/2→6H13/2 transitions, respectively. Commission Internationale de L'Eclairage and correlated color temperature data confirmed their cool-white emission under ultraviolet excitation,this can be used as a white light-emitting diodes due to their luminescentproperties[27].

[18] Wankassama Haron.et.al. were synthesized nanocrystalline LaMO3 (M = Al, Fe, Co, Gd) perovskites by the co-precipitation method using carbonate salts and metal nitrate as starting materials. The products were characterized via XRD,EDX,SEM,TEM,BET and DRS. The XRD patterns confirmed the formation of the perovskite phase. The SEM micrographs indicated that perovskite samples were nano- sized particles with morphology containing porosity due to inter- particle voids. The measured pHpzc of LaAlO3, LaCoO3, LaFeO3, and LaGdO3 were 8.6, 9.2, 9.0, and 8.1, respectively.The DRS spectra, the band gap energies of LaAlO3, LaCoO3, LaFeO3, and LaGdO3 were calcu-lated as 2.60, 1.50, 2.00, and 2.90 eV, respectively. The preparation of LaMO3 (M = Al, Fe,Co, Gd) perovskites have several advantages such as no waste,simplicity,low cost compared with other methods[28].

[19] Prashant K.Sahu.et.al. was synthesized $LaAlO_3$ by gelation–precipitation techniqueusing low cost inorganic precursors. The SEM and TEMs how that powders have a regular and spherical morphology. Phase evolution, morphology, agglomeration and surface area were stud-ied as a function of chloride content and heat treatment temperature. The samples containing chloride crystallized at 1100◦C with the formation of intermediate phases. The product was highly agglomerated and had low surface area. The as-synthesized chloride-free samples crys- tallized directly to pure LaAlO3 perovskite phase at 600◦C,which is the lowest crystallization temperature achieved so far.SEM and TEM of chloride-free samples reveal very fine clusters of nanosized spherical particles.As synthesized and calcined chloride-free samples have a high sur-face area and are thermally stable upto 1600◦C without decomposition. The low temperature phase formation in the precipitated chloride free powders is due to very small particle size of the precipitate and the absence of any intermediate phases during the heat treatment process, so that LaAlO3 phase directly forms immediately after the dehydroxylation takes place[29].

Chapter 3: Materials and Methods

In this paper,we used various types of instruments and tools.Fritsch ball milling machine used for Synthesis and deduction of particle size, for XRD analysis we used,for dielectric measurements we used Rigaku-Ultima IV,for dielectric measurements we used Wayne Kerr 6500B, and HITACHI SU8020 used for FESEM analysis are shown below.

3.1 Sample preparation technique

LaALO3 powder were prepared via conventionally method by high energy ball milling. Commercial available powders of lanthanum oxide (La_2O_3) (99.98% Sigma-aldrich), aluminium oxide (Al_2O_3) (99.0% Sigma-aldrich) were used as starting materials.

La0.8Ca0.2AlO3 ceramics were prepared via conventionally method by high energy ball milling. Commercial available powders of Calciaum oxide(CaO),(La2O3) (99.98 % Sigma-aldrich), calcium carbonate (Al2O3) (99.0% Sigma-aldrich) were used as starting materials.

LaALO3 ceramics were prepared via conventionally method by high energy ball milling. Commercial available powders of strontium oxide(SrCO3), (La2O3) (99.98 % Sigma-aldrich), calcium carbonate (Al2O3) (99.0% Sigma-aldrich) were used as starting materials.

The sample was doping via planetary ball milling (Fritsch ball milling) process. In this jar all sample has put into and rotate about 300 rpm for several hours and to get homogeneous mix zirconium ball are use. Several time after some sample are put out into the jar. During ball milling sample carried out for 25h, 50h, 75h, and 100 h. All four samples are send in Furness for calcination. The powder was calcined 900 °C and1 hours stand by, with constant increase rate 3°C/ min each sample for LaAlO3 and LaCaAlO3 nano powders. The powder was calcined 1400 °C and1 hours stand by, with constant increasing rate 3°C/ min each sample for La0.8Sr0.2AlO3 nano poders.Calcinated powders were send in XRD division for finding geometry, and all sample analysed by FESEM, Thermogravimetric Analysis (TGA) Differential Thermal Analysis (DTA). DTA carried out from temperature at 20 to 1200 °C at constant rate of 10 °C/ min of heating in normal atmosphere in a DTG60 analyser . For structure analyser of Calcinated powders performed by XRD (Brukar D8 advance).The X-Ray diffractometer operating at 40 kV and 40 ma with CuK (λ= 1.5418 Å) radiation, with the angle of 10 to 90 ,the steps size of measurement is 0.02 and counting time is 0.1 sec. XRD data was analysed by the Rietveld technique using Panalytical X'part High Score Plus softeare.

3.1.1 Planetary ball milling

Ball milling contains of a hollow cylindrical shell it's rotate about its own axis [fig.1]. The sell axis maybe either horizontal or tilt at a small angle to the horizontal plane. The sell contents partially filled with zirconium balls. The grinding mechanism is done with the ball which may be made of steel, stainless steel or rubber. The length of the meal is approximately equal to its diameter. The ball occupies about 35 to 55 cylindrical shell is usually lined with and corrosion resistant material such as stainless steel or rubber. The diameter of ball use in between 12 mm and 125 mm. the rotating speed of the shell is 52 to 500 rpm and large ball milling the shell maybe 3 meters in diameter and 4.5 m in length. The mechanism of ball milling is when the shell rotates with Zirconium ball high energy impact on the sample and break the sample and uniform grinding particles produced.



Fig.1:- Planetary Ball Milling (Fritsch)

Advantages of Ball Milling

- Low cost of installation.
- Low cost of power consumption.
- Degree of hardness for all sample is suitable.
- It can be used for grinding of certain explosive material which can be used with an inertnormal atmosphere.

Disadvantage of Ball Milling

- It's time taking process and non uniformity in the particle sizes.

3.1.2 Furnace

In this experiment, we explored the use of an electric ignition system in a furnace instead of the traditional pilot light. In a gas-powered burner furnace, the ignition activates a heating element composed of conductive coils. When an electric current passes through these coils, they heat up, with the airflow controlling the temperature. By using a high-heat thermostat, the heating coils are turned on, allowing the furnace to reach temperatures as high as 1400°C in a short amount of time. Specifically, we used a Naskor furnace to heat a sample to 1200°C in a controlled environment. The temperature was increased at a rate of 5°C per minute, held constant for 1 hour, and then allowed to cool down at the same rate.

3.2 Characterization techniques

3.2.1 X-Ray diffractometer (XRD)

According to Bragg's law, X-ray diffraction occurs when the path difference between X-rays reflected from different planes in a crystal lattice is equal to an integer multiple of the wavelength. This leads to constructive interference, resulting in a diffraction peak at a specific angle, θ. By analysing these diffraction peaks, the distances between atomic planes in the crystal (d-spacing) can be determined, which allows for the identification of the crystal structure.In this case, the XRD pattern of the synthesized samples was obtained using Cu Kα radiation with a wavelength of 1.5406 Å. The diffraction peaks in the XRD pattern provide insight into the crystal structure of the material. The law is mathematically expressed as:

$$n\lambda = 2d\sin\theta \quad \text{..... (I)}$$

In this relation **"n"** indicate the order of diffraction or number of planes. And **"d"** is spacing between two consecutive planes," **λ"** is wavelength of x-ray, and "**θ"** is diffraction angle between source and detector of electron beams.

The technique of X-ray line broadening can be used to give information on the particle sizes present in a catalyst sample. This method uses the Scherrer equation:

$$B(2\theta) = K\lambda / L \cdot \cos\theta \quad \text{..... (II)}$$

where the peak width, B(2θ), at a particular value of 2θ (θ being the diffraction angle, λ the X-ray wavelength) is inversely proportional to the crystallite size L; the constant K is a function of the crystallite shape but is generally taken as being about 1.0 for spherical particles. X-ray line broadening gives average values of crystallite size which in most cases agree quite closely with those obtained by TEM; the great advantage of the technique is that the problems of obtaining representative results are less exacting.



The X-Ray diffractometer shown in [fig.2] operating at 40 kV and 40 ma with CuK (λ= 1.5418 Å) radiation, with the angle of 10 to 90 ,the steps size of measurement is 0.02 and counting time is 0.1 sec. XRD data was analysed by the Rietveld technique using Panalytical X'part High Score Plus softeare.

Figure 2: X-Ray Diffratometer (Brukar D8 advance)

3.2.2 FESEM (Field-emission Scanning Electron Microscope)

1. Principle:

- Utilizes a field emission gun (FEG) to generate a high-intensity electron beam.
- Provides high-resolution surface imaging by scanning a sample with this electron beam.

2. Key Features:

- High Resolution: Achieves resolutions down to 1-2 nanometers.
- Low Voltage Operation: Effective at low accelerating voltages, reducing sample damage.
- Magnification: Ranges from 10x to 1,000,000x.

3. Applications:

- Materials Science: Microstructure analysis of metals, ceramics, and polymers.
- Nanotechnology: Imaging of nanoparticles, nanowires, and thin films.
- Biology: Surface examination of cells, tissues, and microorganisms.

Semiconductors: Inspection of microchips and electronic components.

4. Advantages:

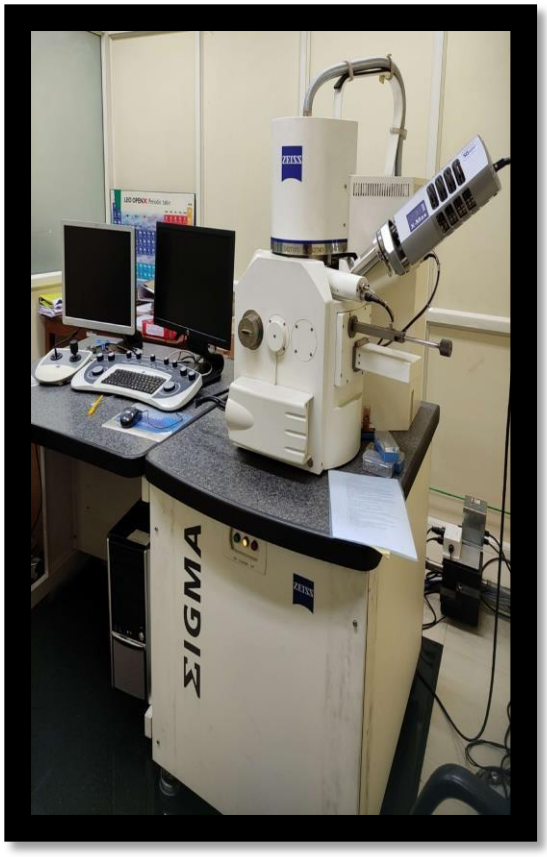
- Superior resolution and image quality.
- Minimal sample preparation, especially for non-conductive materials.
- Versatile across various fields.

5. Limitations:

- High cost and maintenance.
- Samples must be placed in a vacuum environment.
- Some non-conductive samples may require coating.

6. Additional Capabilities:

- Can be paired with Energy Dispersive X-ray Spectroscopy (EDS/EDX) for elemental analysis.



FESEM is essential for detailed surface morphology studies and is widely used in research and industry for its precision and versatility shown in fig.3.

Fig.3.:- Field-Emission Scanning Electron Microscope (FESEM, sigma, Zeiss)

3.2.3 Di-electric Measurement

The dielectric constant (ϵ) of a dielectric material can be defined as the ratio of the capacitance using that material as the dielectric in a capacitor to the capacitance using a vacuum as the dielectric. Typical values of for dielectrics are shown in Table 2.

Table 2 : Dielectric constant of different materials

Material	**Dielectric Constant(ϵ)**
Vacuum	1.000
Dry Air	1.0059
Barium Titanate	100-1250
Glass	3.8-14.5
Quartz	5
Mica	4-9
Water distilled	34-78
Soil dry	2.4-2.9
Titanium dioxide	100

Dielectric constant (ϵ) is given by,

$$\varepsilon = C/C^{o} \ , \ C^{o}=\epsilon^{o} A/t \quad \text{..... (III)}$$

Where,
C = capacitance using the material as the dielectric in the capacitor,
C0 = capacitance using vacuum as the dielectric ϵ^{o} = Permittivity of free space (8.85 x 10-12F/m)
A = Area of the plate/ sample cross section
areat = Thickness of the sample.

3.2.4 TG/DTA analysis

Thermogravimetric analysis (TGA) is a powerful technique for the measurement of thermal stability of materials including polymers. In this method, changes in the weight of a specimen are measured while its temperature is increased. Moisture and volatile contents of a sample can be measured by TGA.DTA measures changes in material where no mass loss occurs. It is also determines endo and exothermic reaction in different temperature, also shows phase transition.

Chapter 4 : Synthesis and characterization of LaAlO3 nano powders.

4.1 Sample preparation

Lanthanum aluminate ($LaAlO_3$) nano powders were prepared via conventionally method by high energy ball milling. Commercial available powders of lanthanum oxide (La_2O_3) (99.98% Sigma-aldrich), aluminium oxide (Al_2O_3) (99.0% Sigma-Aldrich) were used as starting materials .

$$\mathbf{La_2O_3 + Al_2O_3 \rightarrow 2LaAlO_3 + O_2}\ (\uparrow) \quad \textbf{(IV)}$$

La_2O_3=15.2326 gm, Al_2O_3=4.7669 gm of Aldrich sample was taken for this series.

For dielectric measurement, calcinated powders use to determine dielectric constant pressed into pellets at 10 Mpa by hand hydraulic pressed. The diameter was sintered sample is 6mm and thickness is 2 mm. All the pellets are coating with silver pest on both sides for better Conductance. The capacitance and resistance were measure by using Wayne Kerr 6500 Banalyser

4.2 Sample characterizations

Materials with abbreviated sign shown in [fig.3]

Table 3 : Materials with abbreviated sign

Material	Abbreviated
$LaAlO_3$ 25 hours	LAO 25
$LaAlO_3$ 50 hours	LAO 50
$LaAlO_3$ 75 hours	LAO 75
$LaAlO_3$ 100 hour	LAO 100

4.2.1 X-Ray diffractometer (XRD)

The room temperature structures of the LAO samples changing their phases from hexagonal to cubic structure slowly and that is investigated using their respective X-ray (Rigaku Ultimate IV) diffraction profiles. The XRD peaked at 34° which matched the hexagonal structuresof LAO 25 perovskite with JCPDS file shown in [fig.8]. During the Rietveld refinement, we obtained two phases of LaAlO3 (25 hours) one is lanthanum aluminate and another one is lanthanum oxide (La2O3) but lanthanum oxide (La2O3) does not exist in LAO 50,LAO 75 and LAO 100 shown in Table 4. XRD pattern of LAO 25 characterized by small diffraction peaks at 30^0 corresponding to La_2O_3 . The formation of La_2O_3 can be hygroscopic character of lanthanum oxide. The XRD peaks corresponding to γ-Al_2O_3 are not visible due to its amorphous nature shown in [fig.4,fig.5,fig.6,fig.7]. . From the below table we confirmed that LaAlO3 changes their phase from hexagonal to cubic structure slowly.

Table.4: Wt. % of phases, values of Unit cell parameters and Unit Cell volume as obtained by Rietvled Analysis for LaAlO3.

Ball milling hours	25 hrs	50 hrs	75 hrs	100 hrs
Phases	Hexagonal	Hexagonal and Cubic	Hexagonal and Cubic	Cubic
Cell parameter (Å)	a=5.36529 b=5.36529 c=13.12655	a=5.36225 b=5.36225 c=13.14332	a=5.36171 b=5.36171 c=13.13371	a=5.79123 b=5.79123 c=3.79123
Cell Volume (Å^3)	327.2415	327.2882	326.9833	54.4931
Refinement details	GOF=4.78983	GOF=7.29	GOF=1.30899	GOF=1.17788

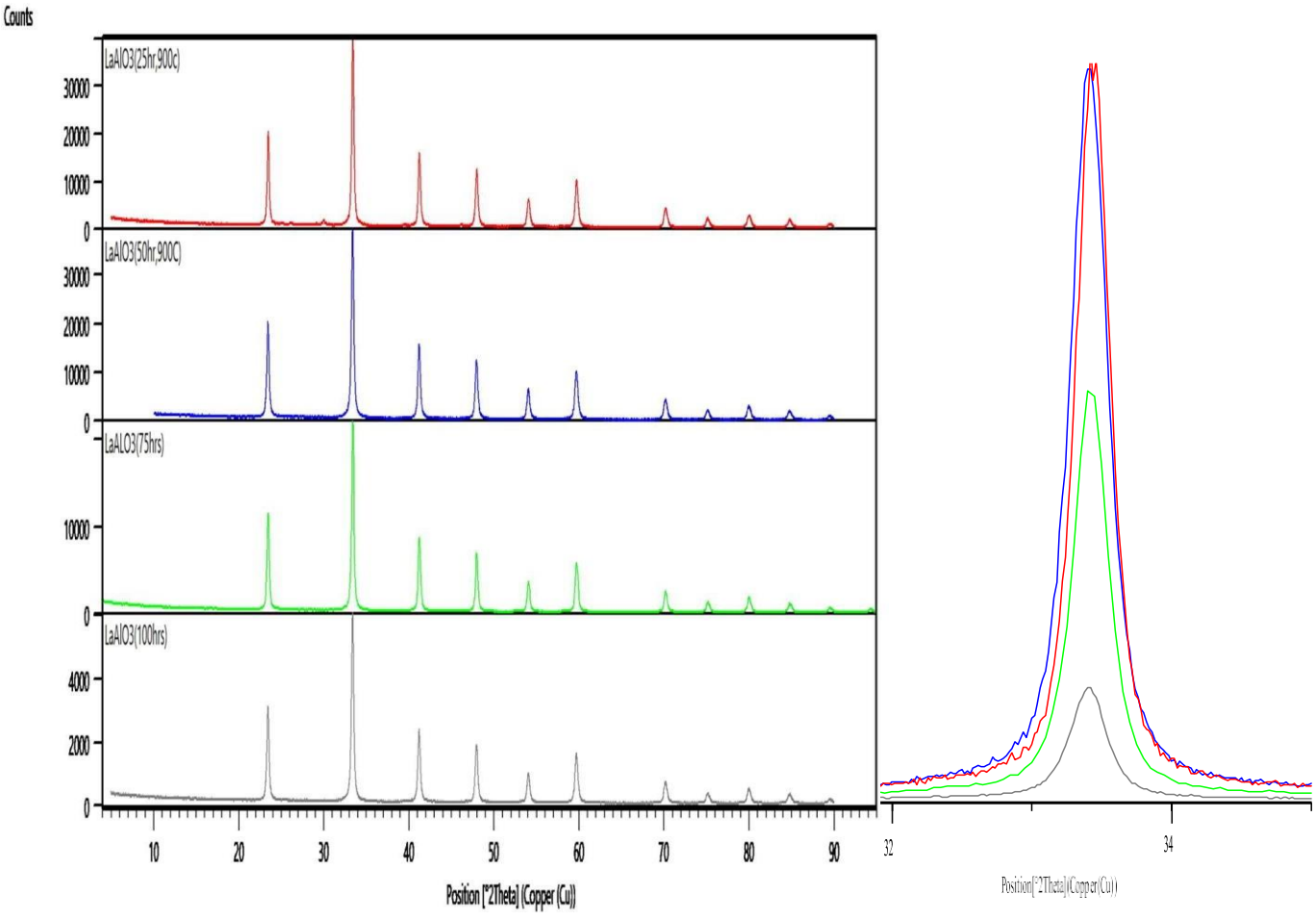


Figure 8: XRD patterns of LAO 25, LAO 50, LAO 75, LAO 100 nano powders.

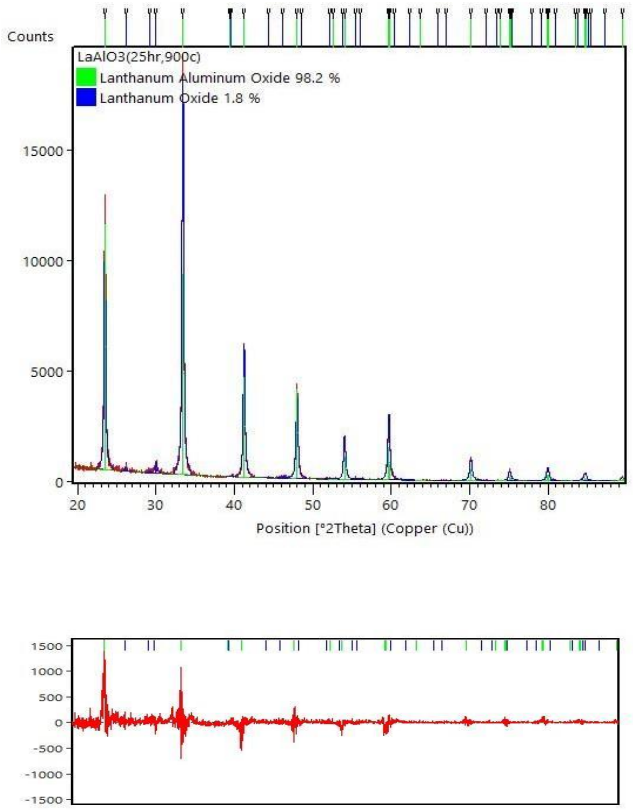


Fig.4:- Rietveld refinement of LAO 25

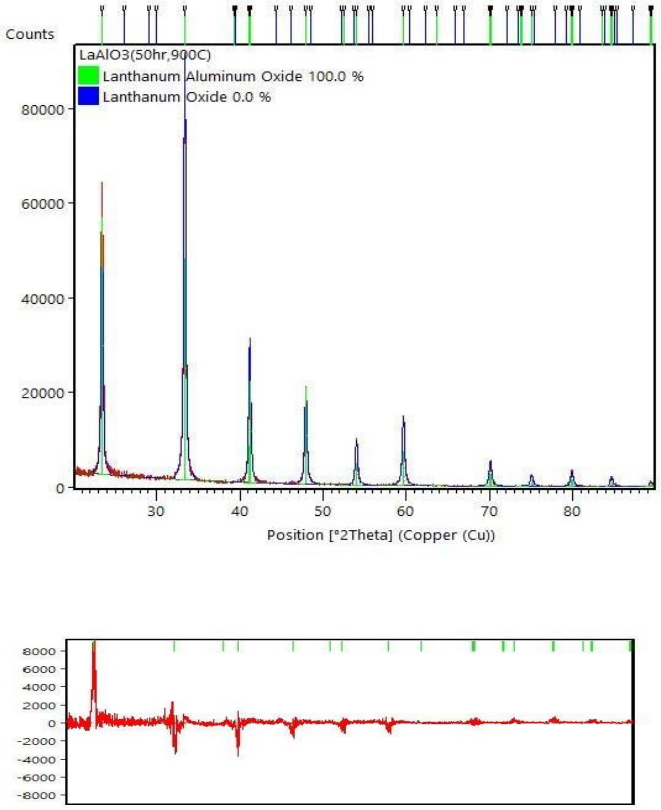


Fig.5:- Rietveld refinement of LAO 50

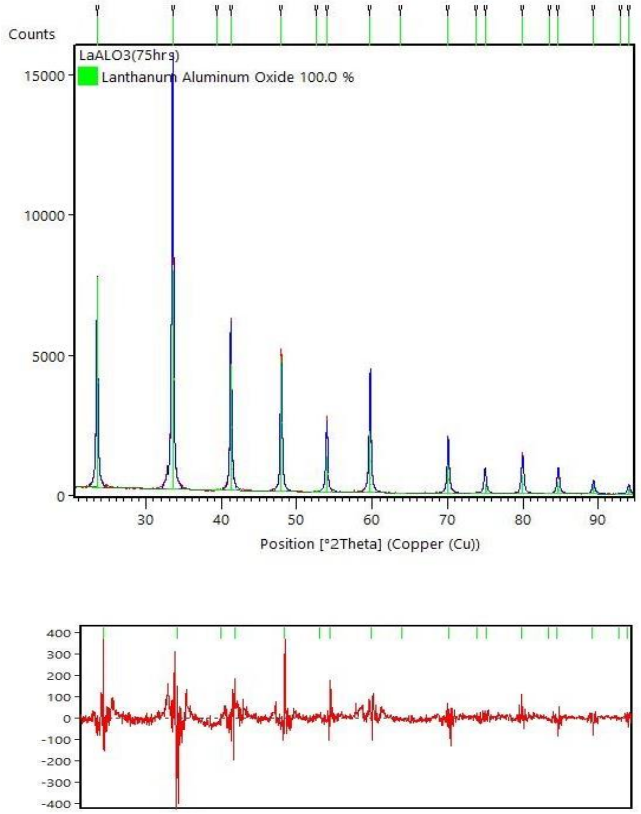


Fig.6:- Rietveld refinement of LAO 75

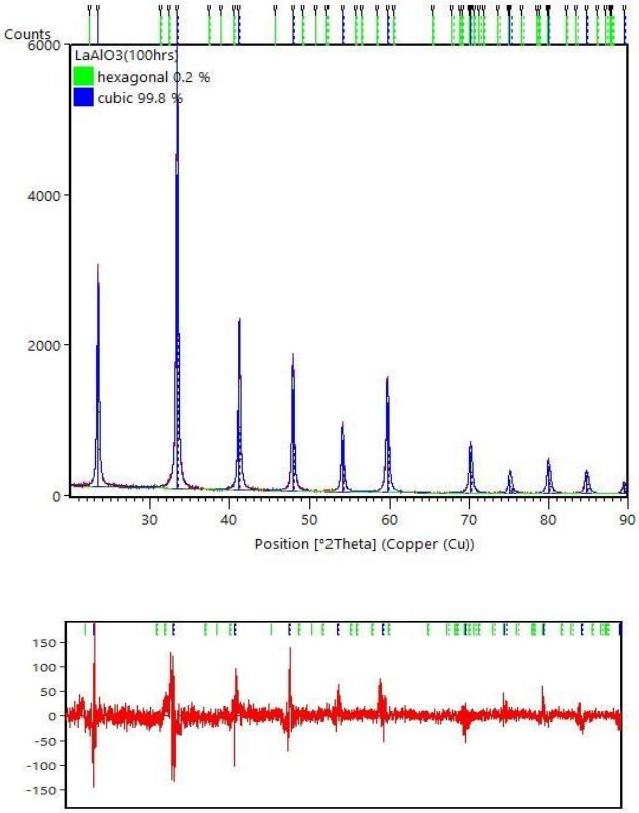


Fig.7:- Rietveld refinement of LAO

In the present study we consider first order (110) reflection for the single profile analysis to calculate crystalline size and lattice strain of this sample. The crystal size and lattice strain was calculated with respect to (110) crystallographic plane which is known as Scherrer formula.

Crystallite size $= \frac{\mathbf{K}\lambda}{\mathbf{B}\cos\theta}$, Lattice strain=$\chi = \frac{\mathbf{B}}{4\tan\theta}$

where, B (size)-B_{obs} -B_{std} & B (strain)- square root (B_{obs}^2-B_{std}^2).

From above equation, B referred as structure broadening, it is the difference between profile width, standard (B_{std}) and the experimental sample (B_{obs}). For single profile analysis standard CLAB6 was used. Because the standard sample did not have any broadening or instrumental broadening in diffractometer. In table 5 shows crystalline size and lattice strain value.

Table.5: Value of crystalline size and lattice strain of LaAlO3 series

Sample	Peak position(2Ɵ) in degree	B_{obs} in degree	B_{std} In degree	Crystallite size(nm)	Lattice Strain(%)
LAO 25	33.4404	0.2903	0.1720	703	0.339
LAO 50	33.4116	0.3184	0.1720	568	0.389
LAO 75	33.4233	0.3011	0.1720	643	0.359
LAO 100	33.4065	0.3111	0.1720	597	0.377

4.2.2 FESEM Analysis

The morphologies of all samples were investigated using field emission scanning electron microscopy (FESEM). Figure [fig.9] shows the FESEM micrographs of the AL2O3, La2O3, LAO 25, LAO 50, LAO 75 and LAO 100. The crystallites with a spherical morphology and size in the range of 50-150nm can be observed. The distribution was confirmed by EDX. Here we clearly see that particle size reduces from 70 nm to 30 nm. The average particle size of LAO 25 is 70.34 nm and LAO 50 is 62.33 nm measures from Histogram plots[fig.10]. Powder gets more agglomerated with increasing ball milling hours. The purity of each sample was also checked with EDX spectrometer (Figure 11). From the EDX pattern, all the elements detected were those that were expected to be present in the samples, i.e. La, Al and O, which affirmed a high purity of the synthesized perovskite .

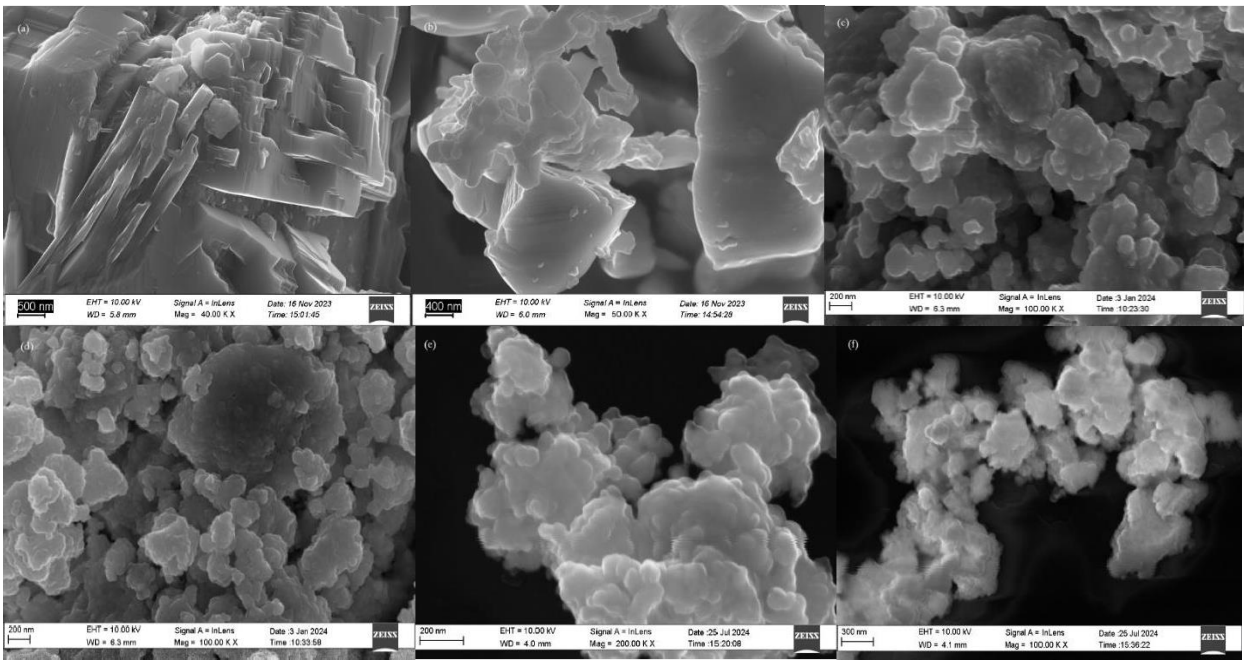


Figure 9: Fesem of (a)Al2O3, (b) La2O3 , (c) LAO 25, (d) LAO 50,(e) LAO 75 and (f) LAO 100 nano powders prepared by ball milling method and calcination at 900°C for 1 Hours.

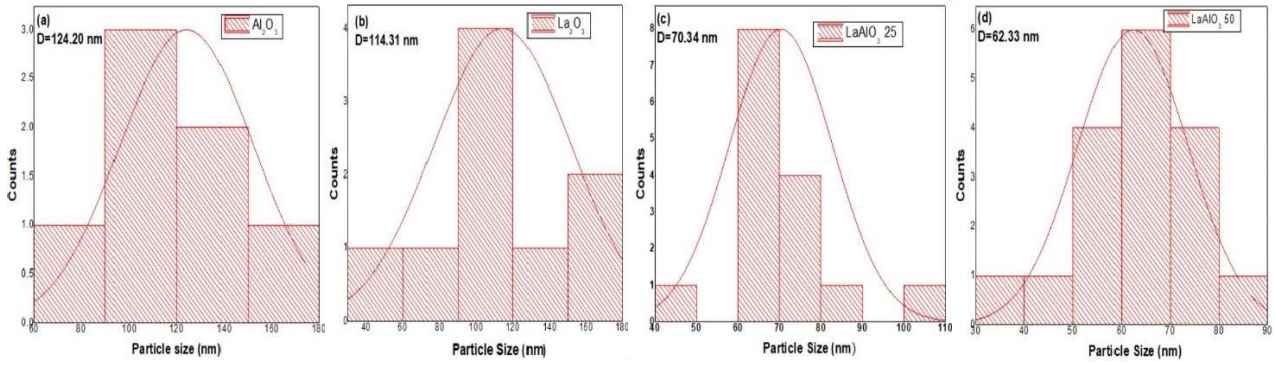


Figure 10: Histogram plots of (a)Al2O3, (b) La2O3 , (c) LAO 25 hrs and (d) LAO 50 nano powders prepared by ball milling method and calcination at 900°C for 1 hr.

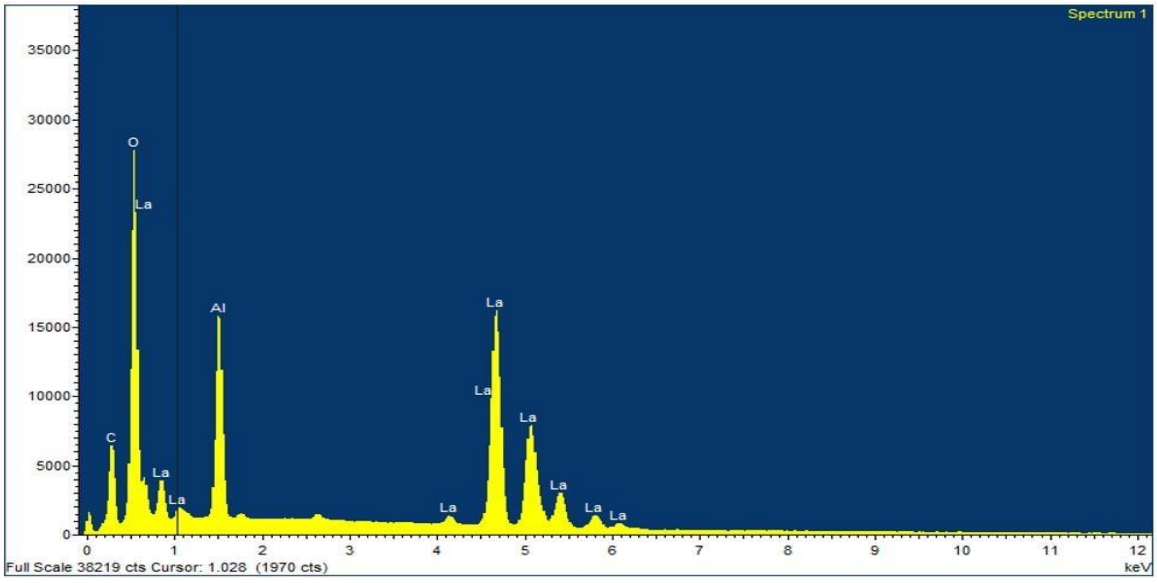


Fig. 11: EDX spectra of LAO

4.2.3Dielectric measurement

This graph confirmed that dielectric constant of LAO series is 30 and capacitance is 2E-12 at high frequency (I MHz). As the particle size decreases with increasing ball milling hours [Fig 12], structural modification is the main reason for changing dielectric properties. As material changes their phase from hexagonal to cubic slowly, so as a result of dielectric constant decreases with ball milling hours. The higher values of dielectric constant at lower frequencies are due to the significant influence of charge relaxation and interfacial polarization. Generally, as frequency increases, the material's overall polarization lags the alternating electric field. Thus, each polarization process stops contributing, decreasing its dielectric constant.

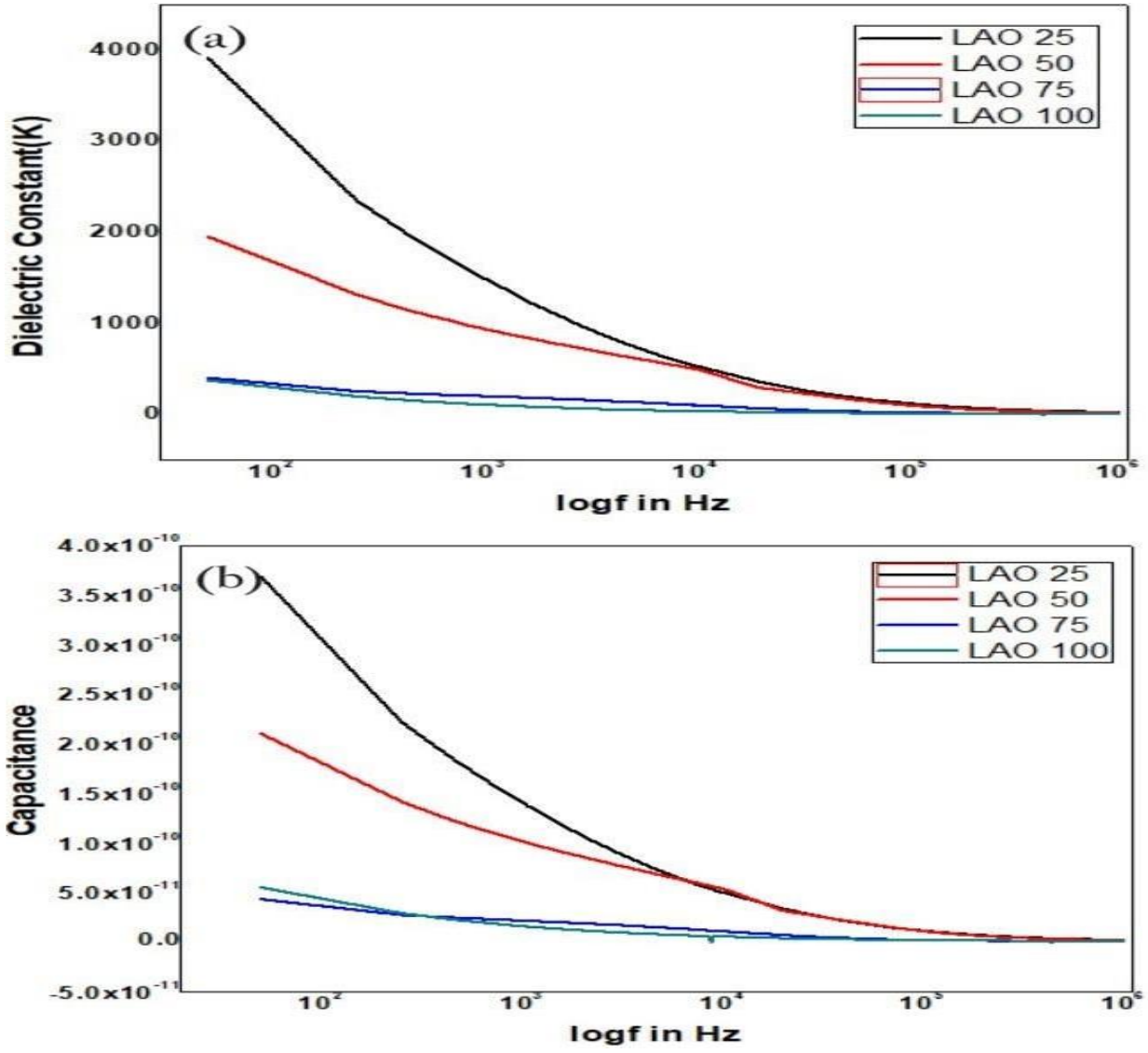


Figure 12: Frequency dependences of the room-temperature dielectric constant and capacitance of LAO 25,LAO 50,LAO 75 and LAO 100 nano powders.

4.2.4 TG/DTA analysis

Figure 13 illustrates the TG/DTA curves of the $LaAlO_3$ nano powders heated at a rate of 5°C/min in the temperature range between 50 and 1000 °C in static air. The TG curve shows the weight loss (4.64%) for $LaAlO_3$ 25, weight loss (-3.54%) for $LaAlO_3$ 50, weight loss (-2.73%) for $LaAlO_3$ 75 and weight loss (-2.39%) for $LaAlO_3$ 100 are mostly due to the decompositionof the oxygen (O2). From fig 13 confirmed that with the reduction of particle size weight loss decreases is mostly due to the gap between nano particles decreases with increasing ball milling hours.

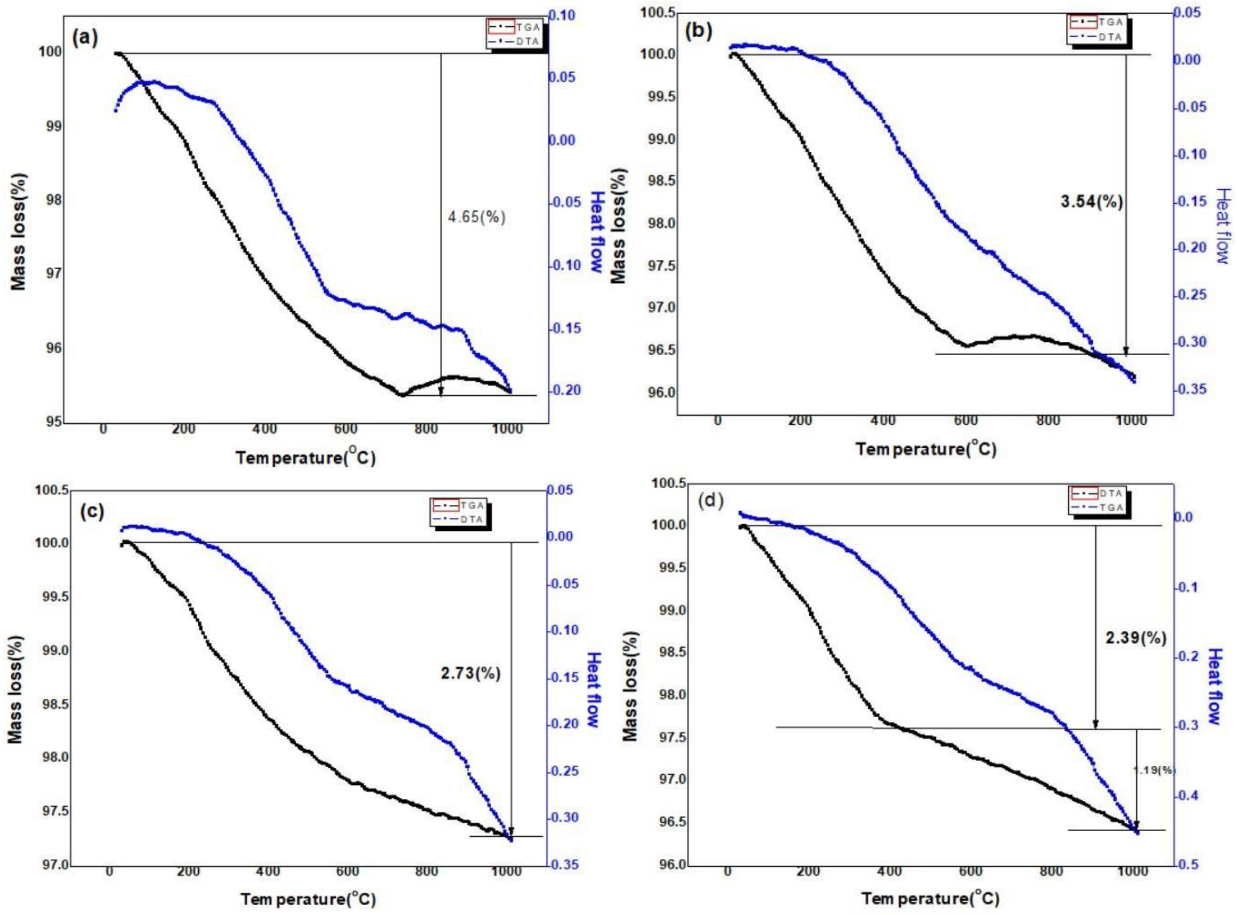


Figure 13: DTA/TG curves of (a)$LaAlO_3$ 25 Hrs, (b) $LaAlO_3$ 50 Hrs(c) $LaAlO_3$ 75 hrs , (d) $LaAlO_3$100 Hrs nano powders with a heating rate of 5°C/min.

Chapter 5 : Synthesis and characterization of Ca doped $LaAlO_3$ ($La_{0.8}Ca_{0.2}AlO_3$) nano powders

5.1 Sample preparation

$La_{1-x}Ca_xAlO_3$ (x=0.2) nanopowders were prepared via conventionally method by high energy ball milling. Commercial available powders of calcium oxide (CaO), lanthanum oxide (La_2O_3) (99.98% Sigma-aldrich), aluminium oxide (Al_2O_3) (99.0% Sigma-aldrich) were used as starting materials.

$0.5(0.2)La_2O_3+0.25CaO +0.5Al_2O_3 \rightarrow La_{0.8}Ca_{0.2}AlO_3+O_2 (\uparrow)$ .....**(V)**

La_2O_3=10.1528 gm, CaO=0.8736 gm,Al_2O_3=3.9716 gm of Aldrich sample was taken for this series.

For dielectric measurement, Calcinated powders use to determine dielectric constant pressed into pellets at 10 Map by hand hydraulic pressed. The diameter was sintered sample is 6mm and thickness is 2 mm. All the pellets are coating with silver pest on both sides for better Conductance. The capacitance and resistance were measure by using Wayne Kerr 6500 Banalyser.

5.2 Sample characterizations

Materials with abbreviated sign shown in [fig.4]

Table 4 : Materials with abbreviated sign

Material	**Abbreviated**
$La_{0.8}Ca_{0.2}AlO_3$ 25 hours	LCAO 25
$La_{0.8}Ca_{0.2}AlO_3$ 50 hours	LCAO 50
$La_{0.8}Ca_{0.2}AlO_3$ 75 hours	LCAO 75
$La_{0.8}Ca_{0.2}AlO_3$ 100 hours	LCAO 100

5.2.1 X-Ray diffractometer (XRD)

This technique is more accurate for determining the amounts of different phases in a material compared to traditional single or multiple profile XRD analysis .The main peaks were attributed to these three phases together with peaks were identified to resemble those of lanthanum oxide La_2O_3, calcium carbonate $CaCO_3$ at about 33° in 2θ attributed to the perovskite oxide were observed. It allows all parameters to be refined at the same time using the least squares method. All parameters (wt% of phases,cell parameter,cell volume and goodness of fitting) are obtained from Rietvled Analysis . In x-ray diffraction pattern Ca replaced La is due to the incorporation of Ca ions with a small ionic radius (1.34 Å) in comparison with La (1.36 Å). From Rietveld refinement, we obtained secondary phase of $CaCO_3$ exist in LCAO 25 and LCAO 50 but not exist in LCAO 75 and LCAO 100 shown in Table 7.

Table.7: Wt. % of phases, values of Unit cell parameters and Unit Cell volume as obtained by Rietvled Analysis in $La_{0.8}Ca_{0.2}AlO_3$.

Ball milling hours	**25 hrs**		**50 hrs**	**75 hrs**	**100 hrs**
Wt % Phases	H^1=76.% O=21.5%		H^1=86.% O=11.1%	H^1	H^1
Parameter (Å)	**H^1**	a=5.36092 b=5.36092 c=13.6988	a=5.3613 b=5..3613 c=13.10686	a=5.36104 b=5.36104 c=13.10237	a=5.36034 b=5.36034 c=13.10401
	O	a=5.076 b=4.717 c=7.504	a=5.076 b=4.717 c=7.504		
Volume (Å^3)	**H^1**	326.0183	326.2596	326.1207	326.0765
	O	179.672	179.672		
Refinement details	GOF =0.95311		GOF =1.10831	GOF =1.22502	GOF =1.2268

H1=Hexagonal phase of $La.8Ca0.2AlO_3$, O=Orthorhombic phase of $CaCO_3$.

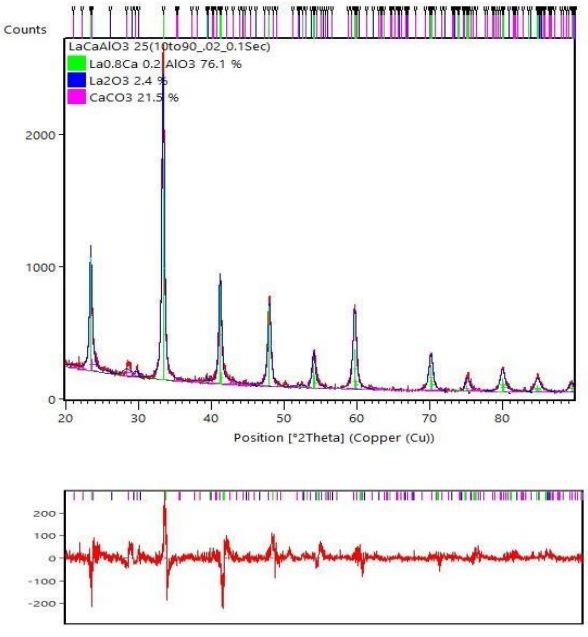


Fig.14:- Rietveld refinement of LCAO(25 hrs)

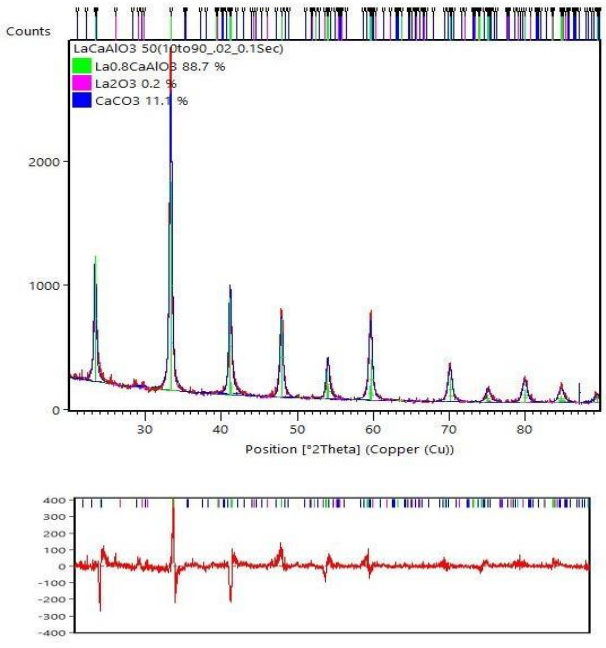


Fig.15:- Rietveld refinement of LCAO(50 hrs)

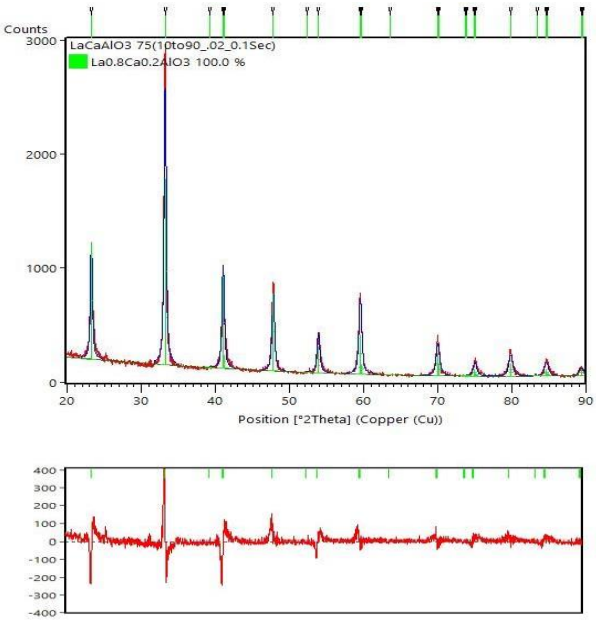


Fig.16:- Rietveld refinement of LCAO (75 hrs)

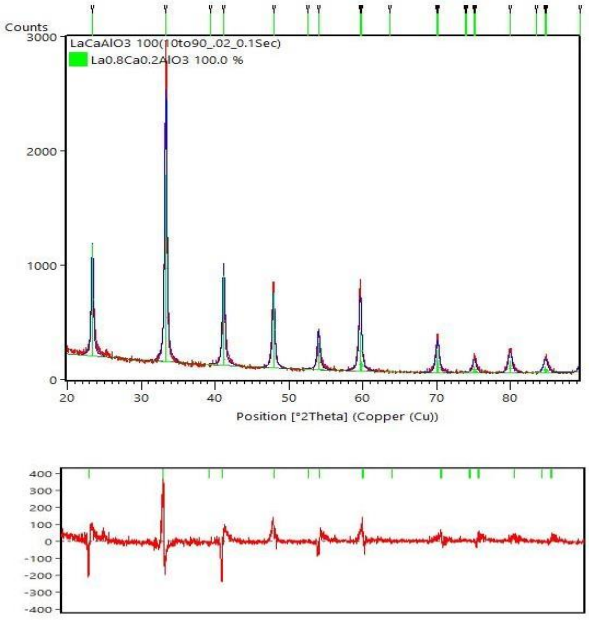


Fig.17:- Rietveld refinement of LCAO (100hrs)

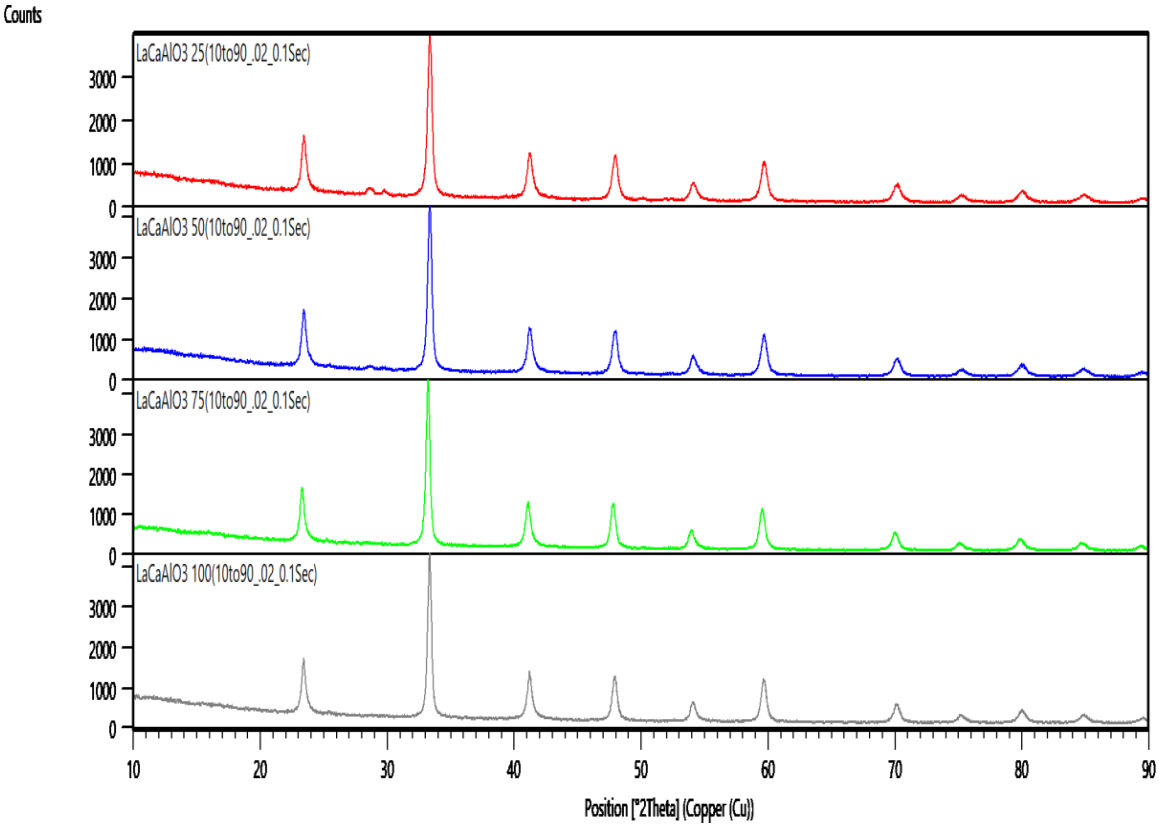


Figure 18:XRD patterns of $La_{0.8}Ca_{0.2}AlO_3$ 25, $La_{0.8}Ca_{0.2}AlO_3$ 50 hrs, $La_{0.8}Ca_{0.2}AlO_3$ 75 hrs and $La_{0.8}Ca_{0.2}AlO_3$ 100 hrs nanocrystallites.

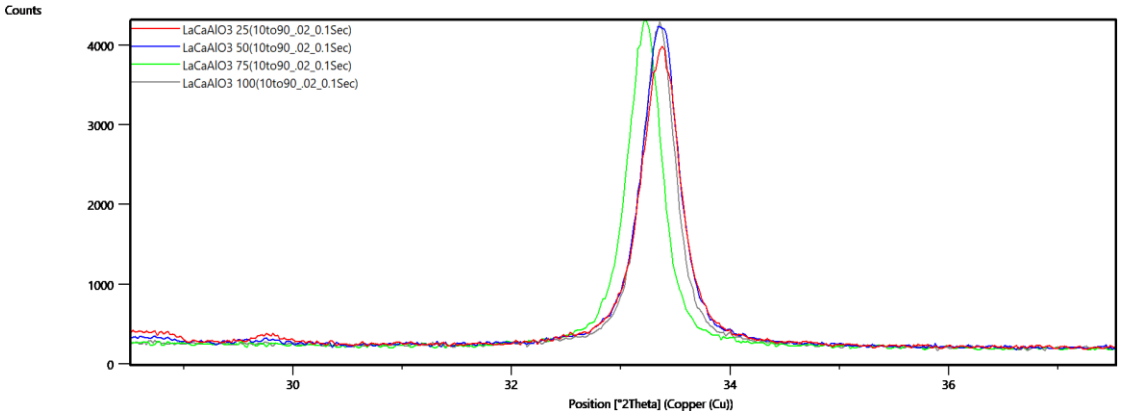


Fig 19. Evolution of the position of the highest X-ray diffraction peak

In the present study we consider first order (110) reflection for the single profile analysis to calculate crystalline size and lattice strain of this sample. The crystal size and lattice strain was calculated with respect to (110) crystallographic plane which is known as Scherrer formula.

$$\text{Crystallite size} = \frac{K\lambda}{B\cos\theta} \quad , \quad \text{Lattice strain} = x = \frac{B}{4\tan\theta}$$

where, B (size)-B_{obs} -B_{std} & B (strain)- square root (B_{obs}^2-B_{std}^2).

From above equation, B referred as structure broadening, it is the difference between profile width, standard (B_{std}) and the experimental sample (B_{obs}). For single profile analysis standard CLAB6 was used. Because the standard sample did not have any broadening or instrumental broadening in diffractometer. In table 8 shows crystalline size and lattice strain value.

Table.8: Value of crystalline size and lattice strain of LCAO series

Sample	Peak position(2Θ) in degree	Bobs In degree	Bstd In degree	Crystallite size(nm)	Lattice Strain(%)
LCAO 25	33.3738	0.4014	0.1720	362	0.527
LCAO 50	33.3669	0.3794	0.1720	401	0.492
LCAO 75	33.2263	0.3583	0.1720	446	0.459
LCAO 100	33.3508	0.3494	0.1720	469	0.442

5.2.2 FESEM analysis

The morphologies of all samples were investigated using field emission scanning electron microscopy (FESEM).[Fig.20] shows the FESEM micrographs of the LCAO 25, LCAO 50, LCAO 75 and LCAO 100. The crystallites with a spherical morphology and size in the range of 40-85 nm can be observed. Powder gets more agglomerated with increasing ball milling hours.The distribution of Ca into LAO was further confirmed by EDX [21]. The purity of each sample was also checked with EDX spectrometer (Figure 21). From the EDX pattern, all the elements detected were those that were expected to be present in the samples, i.e. La, Al, Ca, and O. In addition, all powder samples contained insignificant amounts of other contaminating elements which affirmed a high purity of the synthesized nano powder

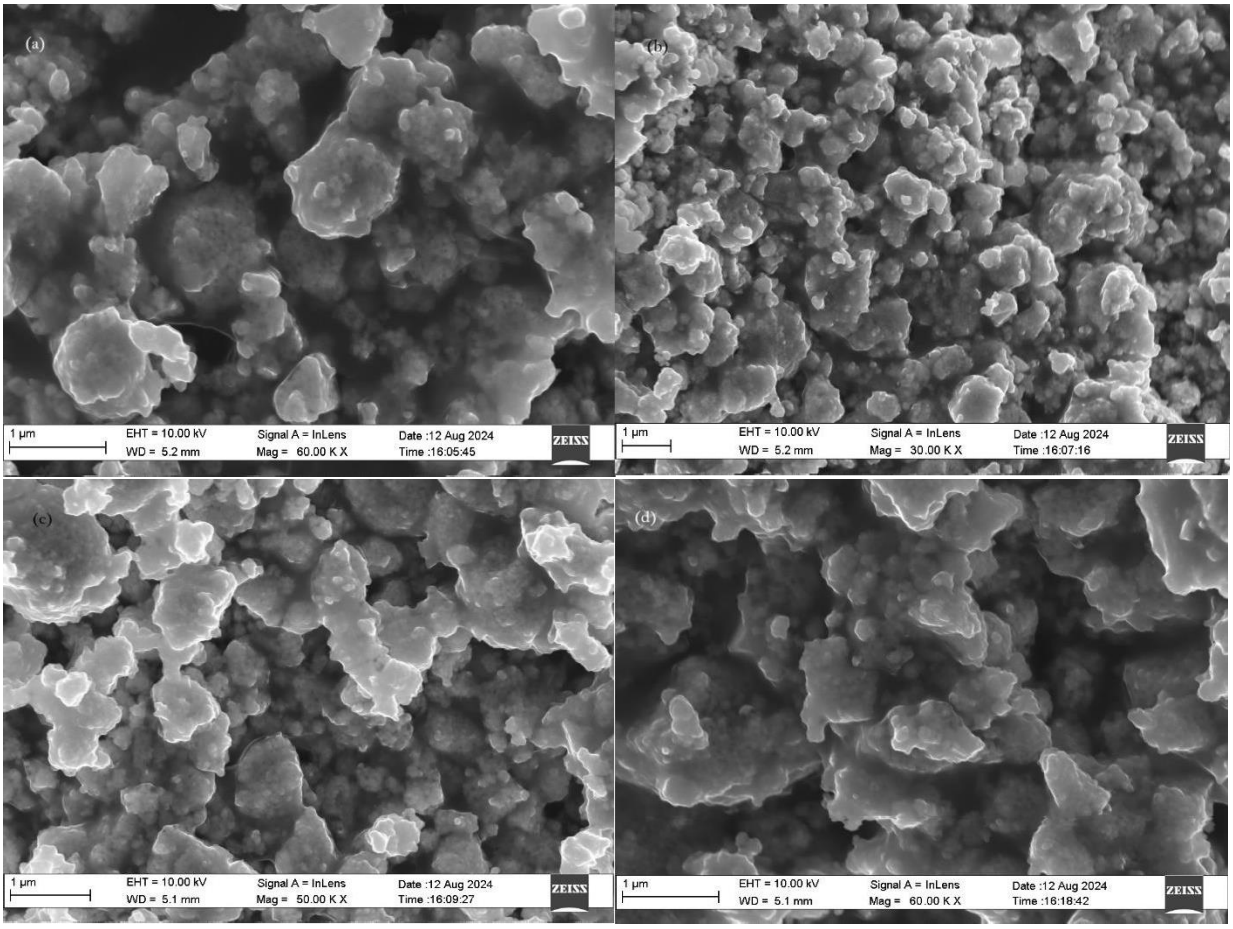


Figure 20: FESEM images of (a) LCAO 25, (b) L C A O 1 0 0 nano powders prepared by ball milling method and calcination at 900°C for 1 hr.

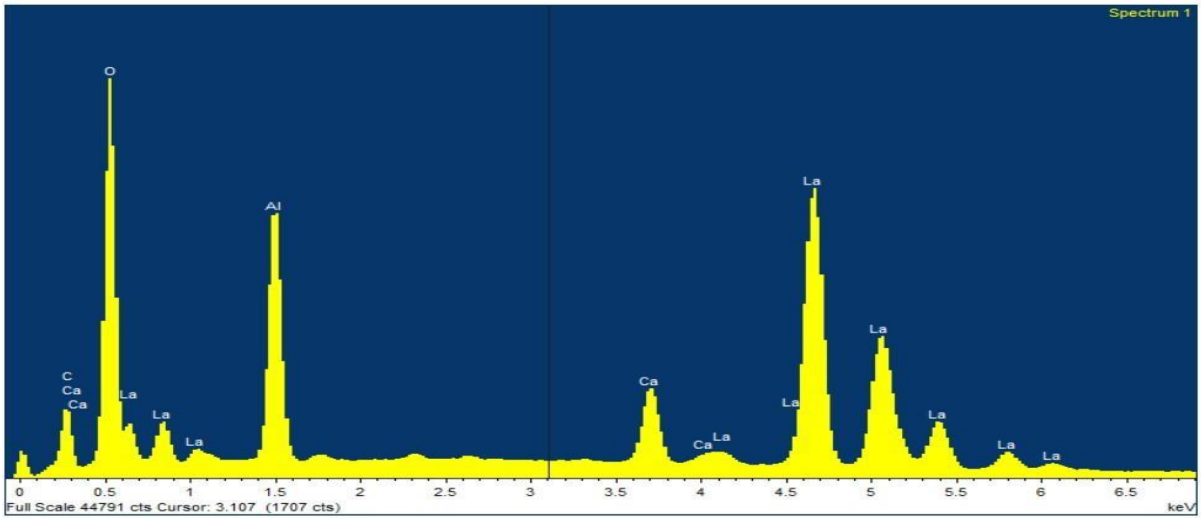


Fig. 21: EDX spectra of LCAO series

5.2.3 Dielectric measurement

This graph confirmed that dielectric constant of LCAO series is 12 and capacitance is 2E-12 at high frequency (I MHz). As the particle size decreases with increasing ball milling hours [Fig 22]. Structural modification is the main reason for changing dielectric properties. As material changes their phase from hexagonal to cubic slowly and existence of secondary phase (unwanted impurity like CaCO3), so as a result of dielectric constant decreases with ball milling hours. The higher values of dielectric constant at lower frequencies is due to the significant influence of charge relaxation and interfacial polarization. Generally, as frequency increases, the material's overall polarization lags the alternating electric field. Thus, each polarization process stops contributing, decreasing its dielectric constant.

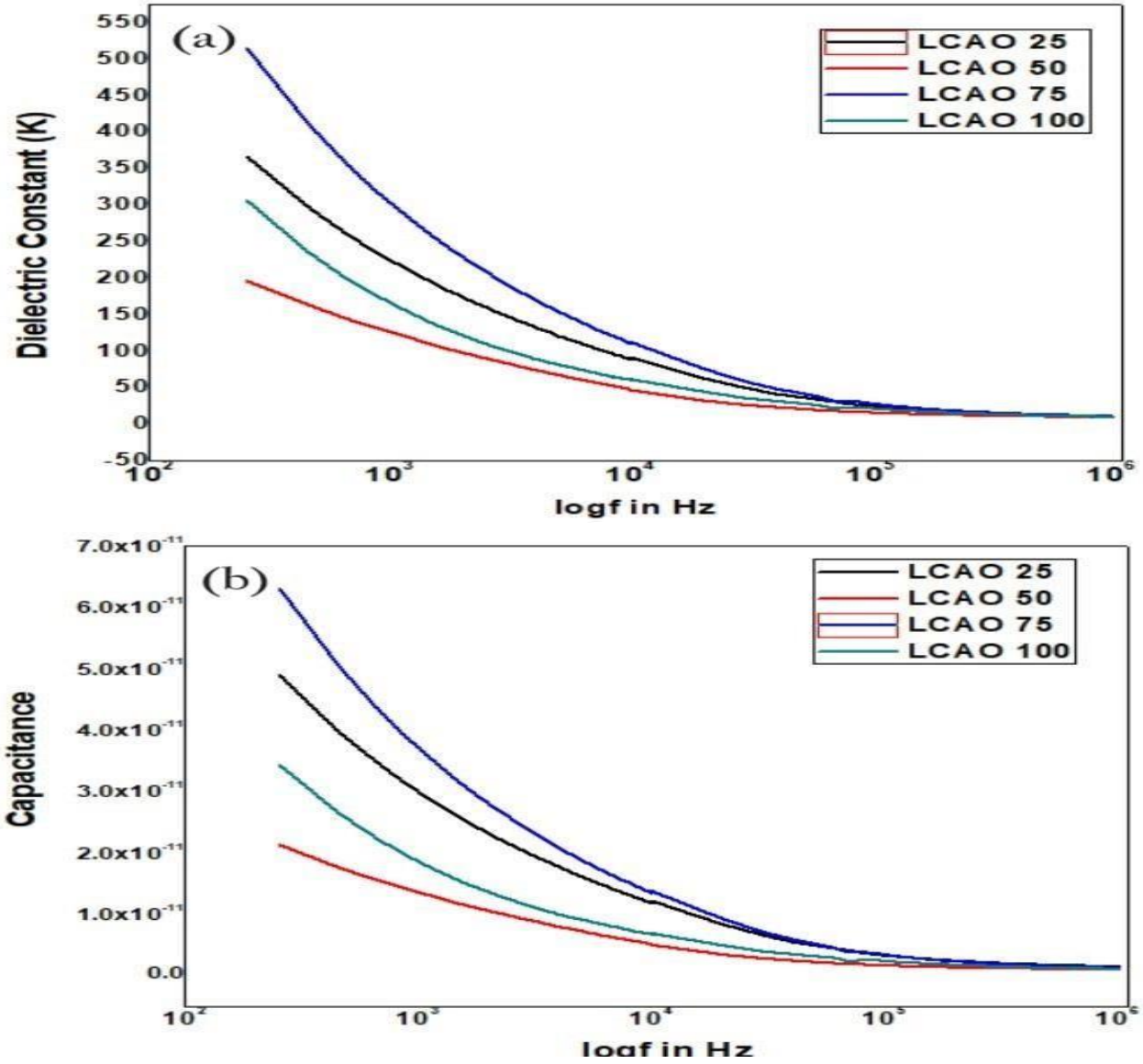


Figure 22: Frequency dependences of the room-temperature dielectric constant and capacitance of LCAO 25, LCAO 50, LCAO 75 and LCAO 100 nano powders.

5.2.4 TG/DTA analysis

Figure 23 illustrates the TG/DTA curves of the LCAO nano powders heated at a rate of 5°C/min in the temperature range between 50 and 1000 °C in static air. The TG curve shows the weight loss (4.63%) for LCAO 25, weight loss (-3.35%) for LCAO 50, weight loss (-2.7%) for LCAO 75 and weight loss (-2.25%) for LCAO 100 are mostly due to the decompositionof the oxygen(O2). From fig 6 confirmed that with the reduction of particle size ,weight loss decreases is mostly due to the gap between nano particles decreases with increasing ball milling hours.

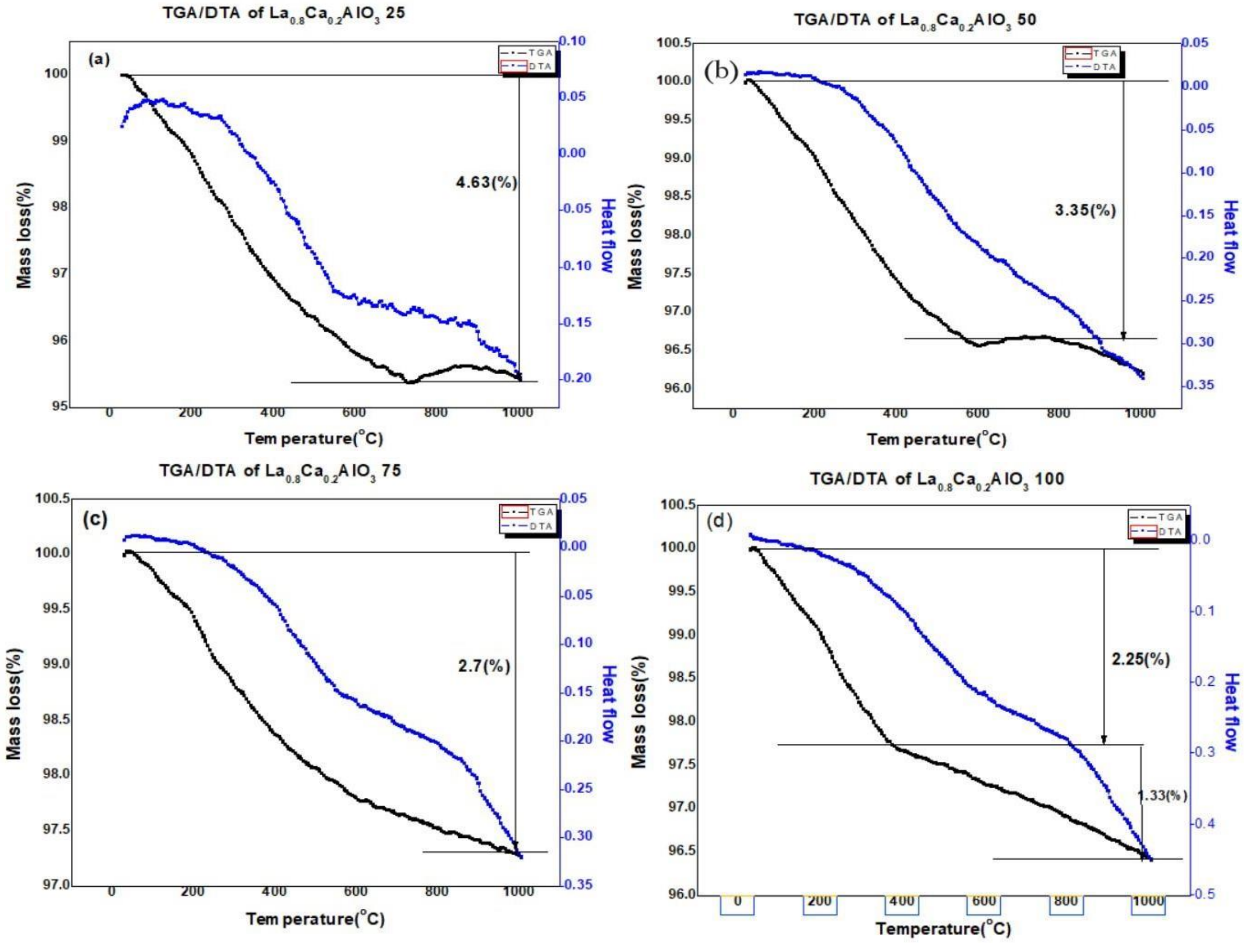


Figure 23: TG/DTA of (a) LCAO 25, (b) LCAO 50 , (c) LCAO75 , (d) LCAO 100 nano powders prepared by ball milling method and calcination at 900°C for 1 hours.

Chapter 6 :Synthesis and characterization of Sr doped LaAlO3 ($La_{0.8}Sr_{0.2}AlO_3$) nano powders

6.1 Sample preparation

$La_{0.8}Sr_{0.2}AlO_3$ nanopowder were prepared via conventionally method by high energy ball milling. Commercial available powders of strontium carbonate ($SrCO_3$), lanthanum oxide (La_2O_3) (99.98% Sigma-aldrich), aluminium oxide (Al_2O_3) (99.0% Sigma-aldrich) were used as starting materials.

$0.5(0.2)La_2O_3+0.2SrCO_3 +0.5\ Al_2O_3 \rightarrow La_{0.8}Sr_{0.2}AlO_3 +CO_2(\uparrow)$ ..... **(VI)**

La_2O_3=9.6 gm, Al_2O_3= 3.75 gm, $SrCO_3$=2.17 gm of Aldrich sample was taken for this series.

For dielectric measurement, calcinated powders use to determine dielectric constant pressed into pellets at 10 Mpa by hand hydraulic pressed. The diameter was sintered sample is 6mm and thickness is 2 mm. All the pellets are coating with silver pest on both sides for better Conductance. The capacitance and resistance were measure by using Wayne Kerr 6500 Analyzer.

6.2 Sample characterizations

Materials with abbreviated sign shown in [fig.9]

Table 9 : Materials with abbreviated sign

Material	**Abbreviated**
$La_{0.8}Sr_{0.2}AlO_3$ 25 hours	LSAO 25
$La_{0.8}Sr_{0.2}AlO_3$ 50 hours	LSAO 50
$La_{0.8}Sr_{0.2}AlO_3$ 75 hours	LSAO 75
$La_{0.8}Sr_{0.2}AlO_3$ 100 hours	LSAO 100

6.2.1 X-Ray Diffratometer (XRD) for Phase Analysis

The Rietveld refinement method was used to analyze the crystal structure. This technique is more accurate for determining the amounts of different phases in a material compared to traditional single or multiple profile XRD analysis. It allows all parameters to be refined at the same time using the least squares method. Different parameters (wt% of phases, cell parameter, cell volume and goodness of fitting) are obtained from Rietveld Analysis shown in Table 10. From the below table we confirmed that Sr doped LaAlO3 changes their phase from hexagonal to cubic structure slowly.

Table.10: Wt. % of phases, values of Unit cell parameters and Unit Cell volume as obtained by Rietveld Analysis in $La_{0.8}Sr_{0.2}AlO_3$.

Ball milling hours	**25 hrs**		**50 hrs**	**75 hrs**	**100 hrs**
Wt % and Phases	H^1=100%		H^1=38.8% H^2=61.8%	H1=46% H^2=54%	H^2=100%
Cell parameter (Å)	**H^1**		a=3.7874 b=3.7874 c=3.7874	a=3.79093 b=3.79093 c=3.79093	a=3.79246 b=3.79246 c=3.79246
	H^2	a=5.35946 b=5.35946 c=13.16388	a=5.36296 b=5.36296 c=13.18474	a=5.3578 b=5.3578 c=13.17363	
Cell Volume (Å^3)	**H^1**		327.4985	54.48009	54.54623
	H^2	350.097	54.32807	327.4985	
Refinement details	GOF =2.00916		GOF =2.89556	GOF =2.57	GOF=3.31

H^1=Hexagonal phase of La0.8Sr0.2AlO3.
H^2= Cubic phase of La0.8Sr0.2AlO3

During the Rietveld refinement, we obtained three phases in LSAO 25,LSAO 50, LSAO 75 and LSAO 100 shown in Table 10. Difference plots show that calculate pattern match with experimental data during Rietveld refinement shown in [fig.24, fig.25, fig.26, fig. 27].

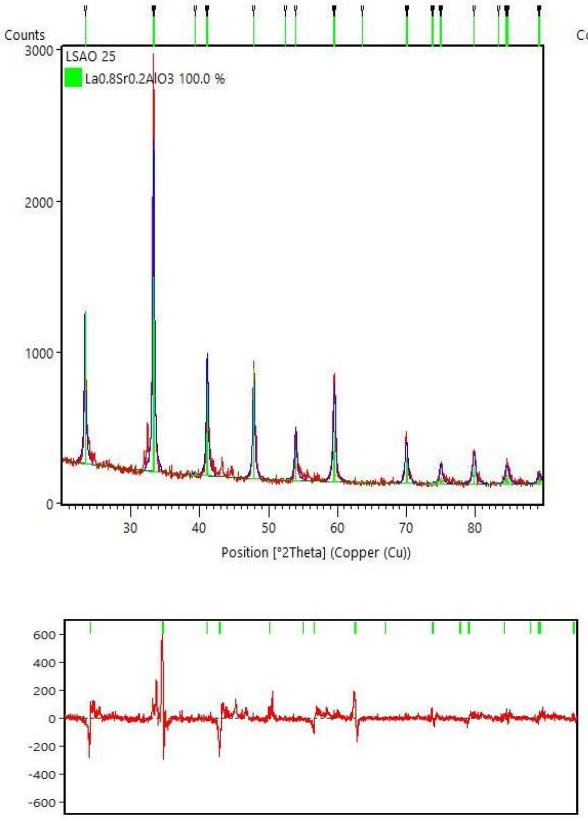


Fig.24:- Rietveld refinement of LSAO 25

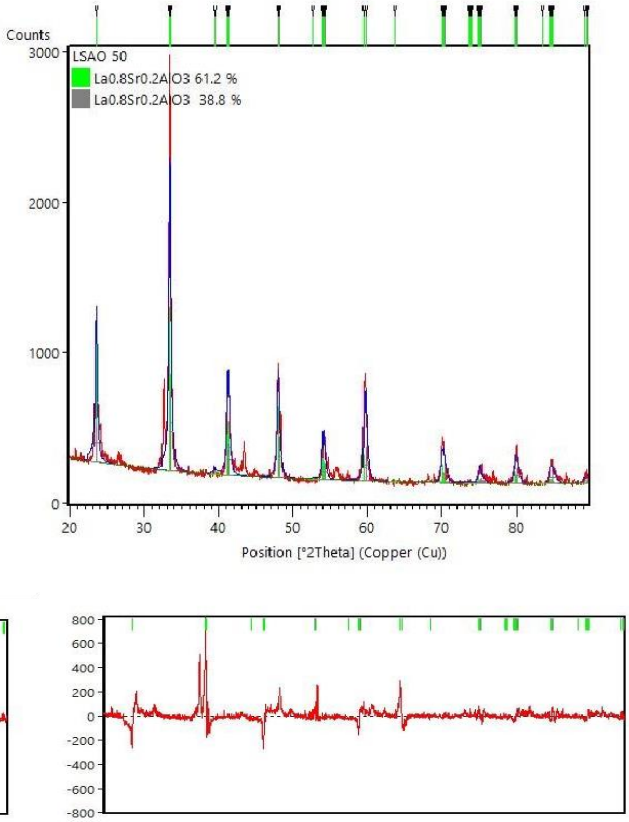


Fig.25:- Rietveld refinement of LSAO 50

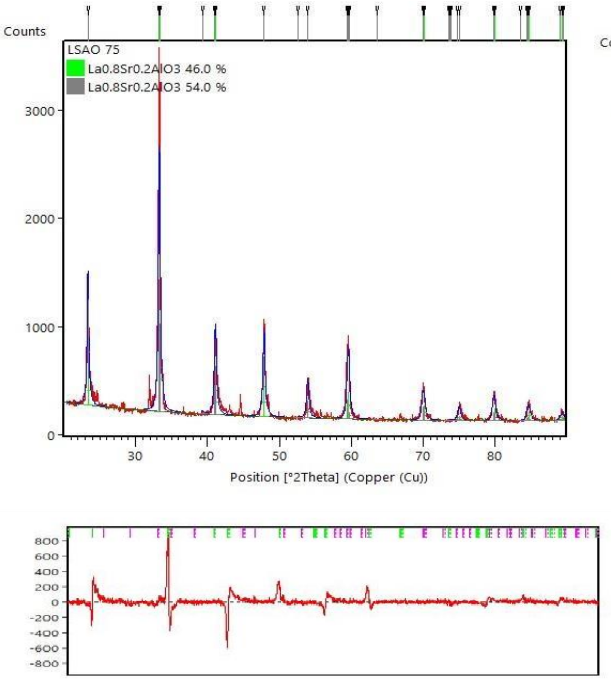


Fig.26:- Rietveld refinement of LSAO 75

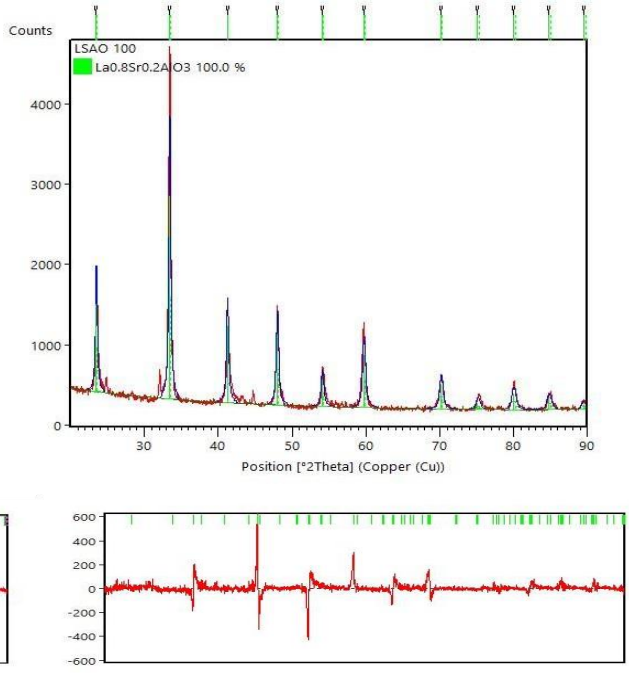


Fig.27:- Rietveld refinement of LSAO 100

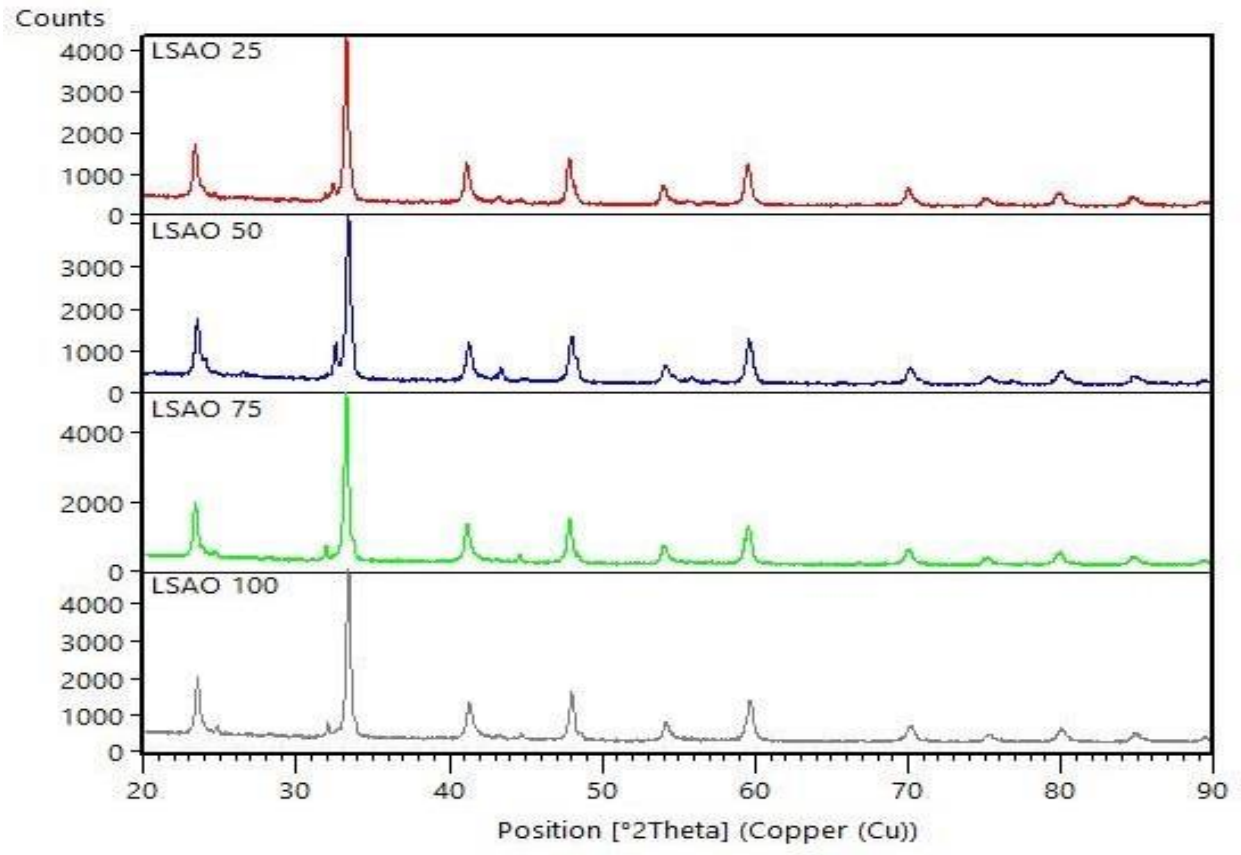


Figure 28:XRD patterns of $La_{0.8}Sr_{0.2}AlO_3$ 25, $La_{0.8}Sr_{0.2}AlO_3$ 50 hrs, $La_{0.8}Sr_{0.2}AlO_3$ 75 hrs and $La_{0.8}Sr_{0.2}AlO_3$ 100 hrs nanocrystallites.

In the present study we consider first order (110) reflection for the single profile analysis to calculate crystalline size and lattice strain of this sample. The crystal size and lattice strain was calculated with respect to (110) crystallographic plane which is known as Scherrer formula.

Crystallite size $= \frac{\mathbf{K}\lambda}{\mathbf{B}\cos\theta}$, Lattice strain=$x = \frac{\mathbf{B}}{4\tan\theta}$

where, B (size)-B_{obs} -B_{std} & B (strain)- square root (B_{obs}^2-B_{std}^2).

From above equation, B referred as structure broadening, it is the difference between profile width, standard (B_{std}) and the experimental sample (B_{obs}). For single profile analysis standard CLAB6 was used. Because the standard sample did not have any broadening or instrumental broadening in diffractometer.

6.2.2 FESEM analysis

The morphologies of all samples were investigated using field emission scanning electron microscopy (FESEM). [Fig.29] shows the FESEM micrographs of the LSAO series. Powder gets more agglomerated with increasing ball milling hours. The distribution of Sr into LAO was further confirmed by EDX [30]. From EDX pattern, all the elements detected were those that were expected to be present in the samples, i.e. La, Al, Sr, and O. In addition, all powder samples contained insignificant amounts of other contaminating elements which affirmed a high purity of the synthesized nano powder.

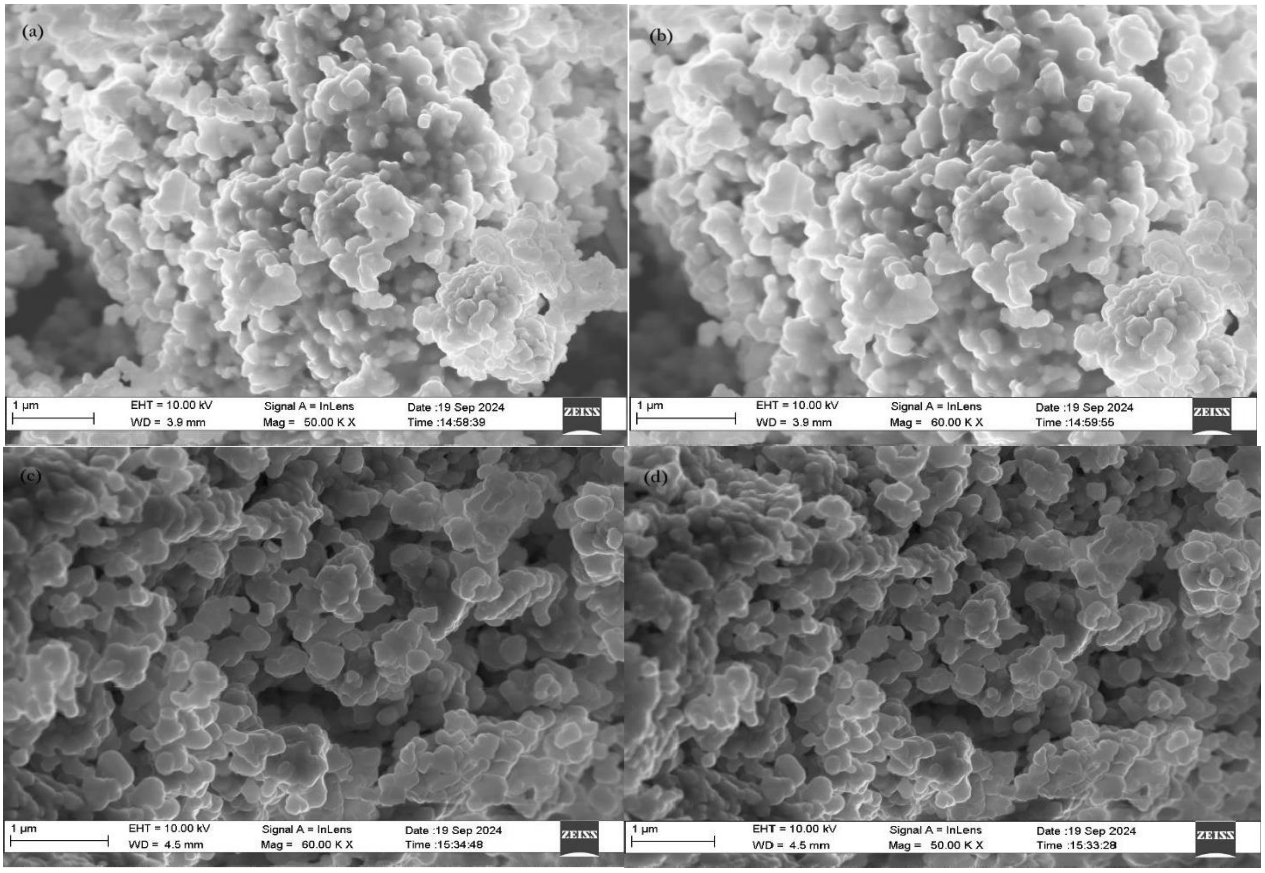


Figure 29: FESEM images of (a), (b) LSAO 25 a n d (c), (d) L S A O 1 0 0 nano powders prepared by ball milling method and calcination at 900°C for 1 hr.

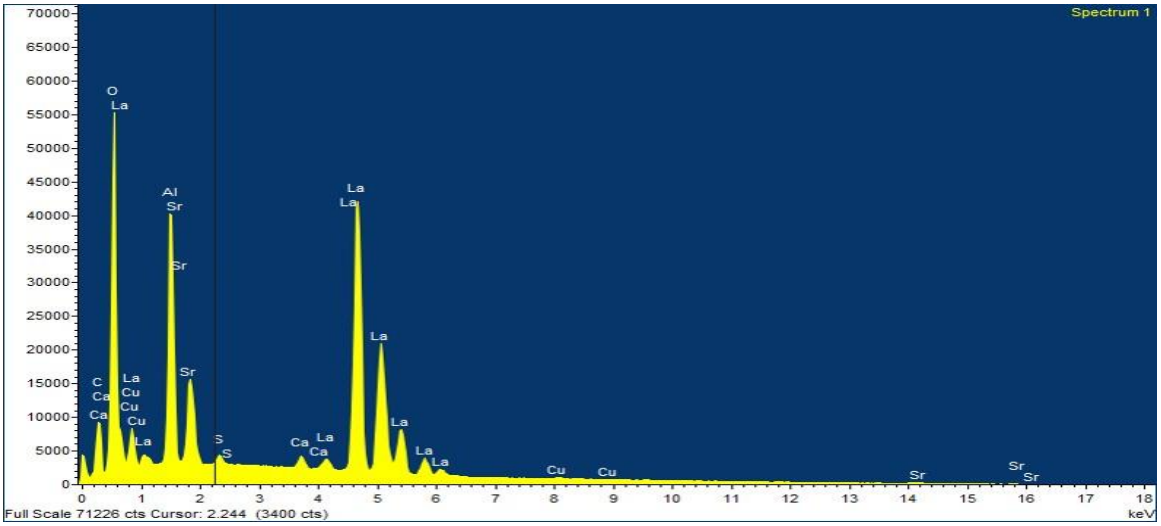


Fig. 30: EDX spectra of LSAO series

6.2.2 Dielectric Measurements

This graph confirmed that dielectric constant of LCAO series is 12 and capacitance is 2E-12 at high frequency (I MHz). Particle size decreases with increasing ball milling hours [Fig 22]. Structural modification is the main reason for changing dielectric properties. LSAO material changes their phase from hexagonal to cubic slowly and existence of secondary phase (unwanted impurity), so that's why capacitance and dielectric constant decreases with ball milling hours. The higher values of dielectric constant at lower frequencies are due to the significant influence of charge relaxation and interfacial polarization. Generally, as frequency increases, the material's overall polarization lags the alternating electric field. Thus, each polarization process stops contributing, decreasing its dielectric constant.

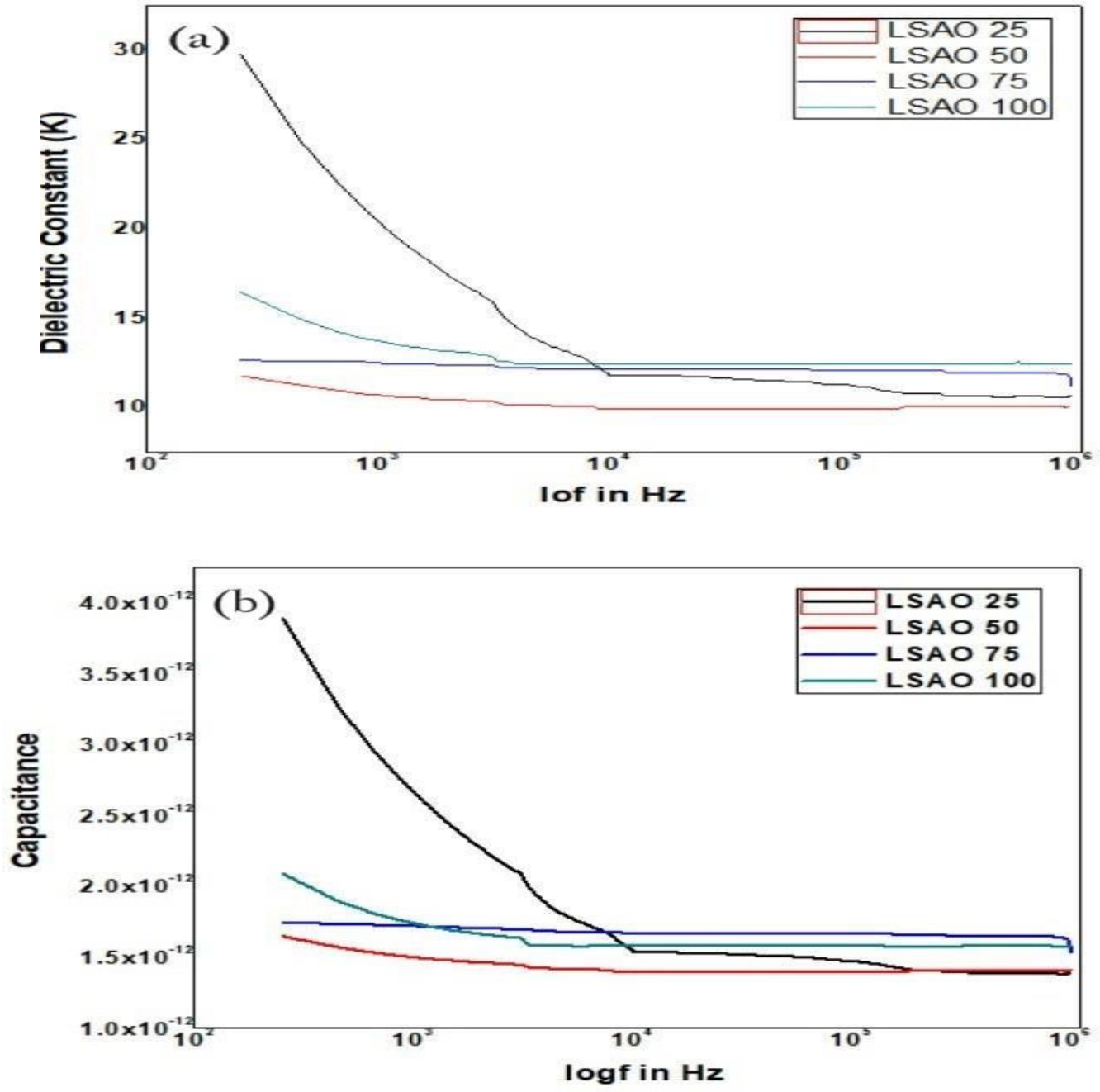


Figure 31: Frequency dependences of the room-temperature dielectric constant and capacitance of LSAO 25, LSAO 50, LSAO 75 and LSAO 100 nano powders.

6.2.3 TG/DTA analysis

Figure 32 illustrates the TG/DTA curves of the LSAO nano powders heated at a rate of 5°C/min in the temperature range between 50 and 1000 °C in static air. The TG curve shows the weight loss (4.63%) for LSAO 25, weight loss (-3.35%) for LSAO 50, weight loss (-2.7%) for LSAO 75 and weight loss (-2.25%) for LSAO 100 are mostly due to the decompositionof the oxygen(O2). From fig 6 confirmed that with the reduction of particle size ,weight loss decreases is mostly due to the gap between nano particles decreases with increasing ball milling hours.

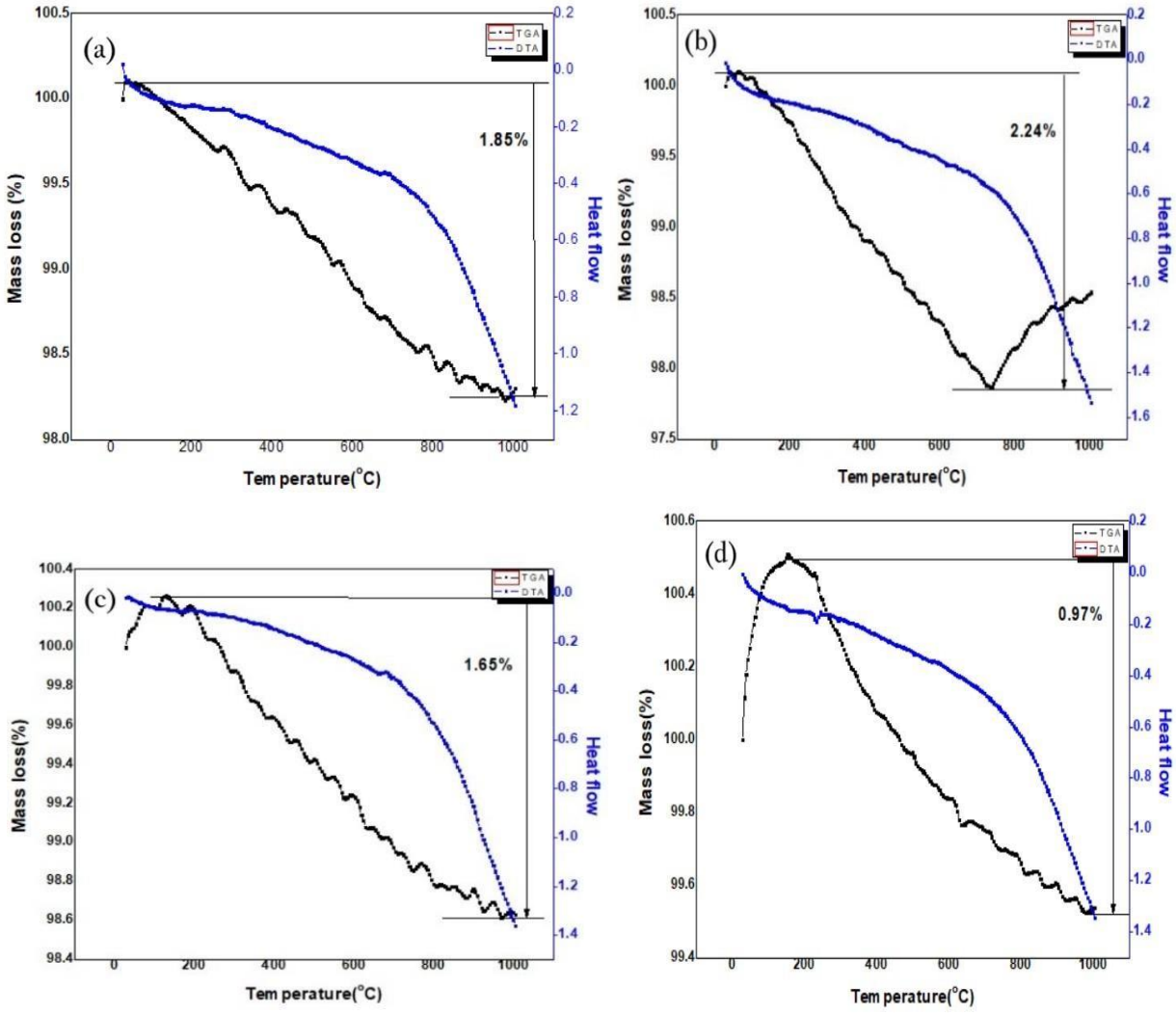


Figure 32: TG/DTA of (a) LSAO 25, (b) LSAO 50 , (c) LSAO 75 , (d) LSAO 100 nano powders prepared by ball milling method and calcination at 900°C for 1 hours.

Chapter 7: Conclusion

In this study, $LaAlO_3$, Ca doped $LaAlO_3$ and Sr doped $LaAlO_3$ perovskites have been successfully prepared by High energy ball milling process. X-Ray diffraction (XRD) confirmed that $LaAlO_3$ and Ca or Sr doping introduces multiple phases, here multiphases transform to single phase with increase ball milling time. XRD also confirmed that $LaAlO_3$ samples changing their phase from hexagonal to cubic structure slowly with increasing ball milling hours. TG/DTA confirmed that with the reduction of particle size weight loss decreases is mostly due to the gap between nano particles decreases with increasing ball milling hours. Field-emission Scanning Electron Microscopy (FESEM) shows that LaAlO3 consists fine clusters of nanosized spherical particles and it gets highly agglomerated with increasing ball milling hours. The dielectric constant of $LaAlO_3$ ranges from 30 to 12, with the dielectric properties influenced by the local atomic arrangement of Ca and Sr atoms and the coexistence of multiple phases.

For LCAO series, dielectric constant decreases with respect to LaAlO3 a nd dielectric constant decreases from 30 to 12 at high (1Mhz) frequencies. It was observed from Rietveld analysis that Ca doped $LaAlO_3$ shows existence of secondary phase (unwanted impurity $CaCO_3$) which play vital role in dielectric measurement. so as a result of dielectric constant decreases with ball milling hours. FESEM reported that it consists of fine clusters of nanosized spherical particles and it gets agglomerated with increasing ball milling hours. From TG/DTA we confirmed that mass loss is very small amount.

For LSAO series, dielectric constant decreases with respect to LaAlO3 and Ca doped LaAlO3 and dielectric constant is 10. Rietveld analysis shows that it transforming phase from hexagonal to cubic phase. From TG/DTA we confirmed that mass loss is very small amount. FESEM reported that it consists of fine clusters of nanosized spherical particles and it gets agglomerated with increasing ball milling hours. Even a tiny amount of dopant, such as Sr or Ca, can significantly alter the material's electrical conductivity and dielectric constant. This study focuses on how the Dielectric properties of $LaAlO_3$ powder changes with particle size reduction and aims to correlate these structural changes with dielectric properties at the nanoscale, given the trend toward miniaturization in electronic devices.

References

[1] Mahmoud Nasrollahzadeh, S. Mohammad Sajadi, Mohaddeseh Sajjadi, Zahra Issaabadi, Chapter 1 – "An Introduction to Nanotechnology", Editor Atarod,Interface Science and Technology,Elsevier,Volume 28,2019,

[2] Bayda S, Adeel M, Tuccinardi T, Cordani M, Rizzolio F. The History of Nanoscience and Nanotechnology: From Chemical-Physical Applications to Nanomedicine. Molecules. 2019

[3] Ibrahim Khan, Khalid Saeed, Idrees Khan, Nanoparticles: Properties, applications and toxicities, Arabian Journal of Chemistry, Volume 12, Issue 7,2019

[4] Parappurath N. Sudha, Kirubanandam Sangeetha, Kumar Vijayalakshmi, Ahmed Barhoum,Chapter 12 - Nanomaterials history, classification, unique properties, production and market, ,Elsevier,2018

[5] Muhammad Rizwan1, Samina Gul1, Tahir Iqbal5,1, Uzma Mushtaq2, M Hassan Farooq3, Muhammad Farman4, Rabia Bibi1 and Mohsin Ijaz5, "A review on perovskite lanthanum aluminate (LaAlO3), its properties and applications "Materials Research Express, Volume 6,2019

[6] Bryan C. Chakoumakos,D. G. Schlom,Michael Urbanik,J. Luine, "Thermal expansion of LaAlO3 and (La,Sr)(Al,Ta)O3, substrate materials for superconducting thin-film device applications" Journal of Applied Physics

[7] Ranjithkumar Bheemaraj,Dr. Sathish sugumaran,D.Nadaraj et.al. "Structural and electrical properties of LaAlO3 nanoparticles" International Journal of Biosciences and Nanosciences, Volume, 2014

[8] E.Breckenfeld, Richard B. Wilson " Effect of growth induced (non)stoichiometry on the thermal conductivity,permittivity,and dielectric loss of LaAlO3 ", Applied physics Letters,2013

[9] Yin-Long Han, Sheng-chun shen,Jie You et.al. "Two-dimensional superconductivity at (110) LaAlO3/SrTiO3 interfaces " AIP Publishing,2014

[10] Seung-Kuk Kang, and Hiroshi Ishiwara, " Characteristics of LaAlO3 as insulating buffer layers of ferroelectric -gate field effect transistors" Japanese Journal of Applied Physics,Volume 41,2002

[11] Rizwan, S. Gul, T. Iqbal, U. Mushtaq, M. H. Farooq, M. Farman, R. Bibi, and M. Ijaz, "A review on perovskite lanthanum aluminate (laalo3), its properties and applications," *MaterialsResearch Express*, vol. 6, no. 11, p. 112001, 2019

[12] G.Qin,X.Huang, J. Chen, and Z. He, "Synthesis of sr and mg double-doped laalo3 nanopow- ders via edta-glycine combined process," *Powder technology*, vol. 235, pp. 880–885, 2013.

[13] T. Onishi, "The effects of counter cation on oxide ion conductivity: In the case of sr-doped laalo3 perovskite," *International Journal of Quantum Chemistry*, vol. 110, no. 15, pp. 2912– 2917, 2010.

[14] S. D. Neelapala, N. LAshok Yaranal, and H. Dasari, "Synthesis of la1-xsrxalo3 perovskites by reverse strike co-precipitation method and its soot oxidation activity," *Iranian Journal of Chemistry and Chemical Engineering (IJCCE)*, vol. 38, no. 4, pp. 69–77, 2019.

[15] M. Fabián, B. I. Arias-Serrano, A. A. Yaremchenko, H. Kolev, M. Kaňuchová, and J. Brianˇcin, "Ionic and electronic transport in calcium-substituted laalo3 perovskites prepared via mechanochemical route," *Journal of the European Ceramic Society*, vol. 39, no. 16, pp. 5298–5308, 2019.

[16] J. Zylberberg and Z.-G. Ye, "Improved dielectric properties of bismuth-doped laalo3," *Journal of applied physics*, vol. 100, no. 8, 2006.

[17] J. Yang, Q. Zhang, L. Dong, H. Li, and C. Tian, "Preparation and characterization of si-doped laalo3 solid electrolyte for it-sofcs," *Functional Materials Letters*, vol. 15, no. 07n08, p. 2251056, 2022.

[18] T.-Y. Chen, R.-Y. Pan, and K.-Z. Fung, "Effect of divalent dopants on crystal structure and electrical properties of laalo3 perovskite," *Journal of Physics and Chemistry of Solids*, vol. 69, no. 2-3, pp. 540–546, 2008.

[19] L. A. Villas-Boas, C. A. Goulart, and d. S. D. P. Ferreira, "Effects of sr and mn co-doping on microstructural evolution and electrical properties of laalo3," *Processing and Application of Ceramics*, vol. 13, no. 4, pp. 333–341, 2019.

[20] L. A. Villas-Boas, C. A. Goulart, and D. P. Ferreira de Souza, "Microstructural development and oxygen ion mobility in sr, ba, and ca-doped laalo3 perovskites," *Materia-rio De Janeiro*, p. 10, 2020.

[21] A. H. McDaniel, E. C. Miller, D. Arifin, A. Ambrosini, E. N. Coker, R. O'Hayre, W. C. Chueh, and J. Tong, "Sr-and mn-doped laalo 3- δ for solar thermochemical h 2 and co production," *Energy & Environmental Science*, vol. 6, no. 8, pp. 2424–2428, 2013.

[22] A. V. Egorova, K. G. Belova, I. E. Animitsa, Y. A. Morkhova, and A. A. Kabanov, "Effect of zinc doping on electrical properties of laalo 3 perovskite," *Chimica Techno Acta*, vol. 8, no. 1, p. 20218103, 2021.

[23] J. Y. Park and G. M. Choi, "Electrical conductivity of sr and mg doped laalo3," *Solid State Ionics*, vol. 154, pp. 535–540, 2002.

[24] C. A. da Silva and P. E. V. de Miranda, "Synthesis of laalo3 based materials for potential use as methane-fueled solid oxide fuel cell anodes," *International journal of hydrogen energy*,vol. 40, no. 32, pp. 10 002–10 015, 2015.

[25] A. Zahoor, M. Isa, and T. Mahmood, "Computational study of be doped laalo3 perovskite,"*Physica B: Condensed Matter*, vol. 652, p. 414631, 2023.

[26] L. Djoudi, M. Omari, and N. Madoui, "Synthesis and characterization of lanthanum monoalu - minate by co-precipitation method," in *EPJ web of conferences*, vol. 29. EDP Sciences, 2012, p. 00016

[27] A. Boudali, F. Saadaoui, M. Zemouli, M. D. Khodja, and K. Amara, "Recalculate structural, elastic, electronic, and thermal properties in laalo 3 rhombohedral perovskite," 2013.

[28] P. Kumar, S. Singh, I. Gupta, V. Kumar, and D. Singh, "Luminous laalo3: Dy3+ perovskite nanomaterials: Synthesis, structural, and luminescence characteristics for white light -emitting diodes," *Luminescence*, vol. 37, no. 11, pp. 1932–1941, 2022.

[29] W. Haron, A. Wisitsoraat, U. Sirimahachai, and S. Wongnawa, "A simple synthesis and characterization of lamo 3 (m= al, co, fe, gd) perovskites via chemical co-precipitation method." *Songklanakarin Journal of Science & Technology*, vol. 40, no. 3, 2018.

[30] P. K. Sahu, S. Behera, S. Pratihar, and S. Bhattacharyya, "Low temperature synthesis of microwave dielectric laalo3 nanoparticles: effect of chloride on phase evolution and morphology," *Ceramics international*, vol. 30, no. 7, pp. 1231–1235, 2004.